University of Texas at El Paso
ScholarWorks@UTEP

Open Access Theses & Dissertations

2023-08-01

Geometrical And Surface Texture Characterization For Laser Powder Bed Fusion Process

Jesus Alfredo Rivas
University of Texas at El Paso

Follow this and additional works at: https://scholarworks.utep.edu/open_etd

 Part of the Mechanical Engineering Commons

Recommended Citation

Rivas, Jesus Alfredo, "Geometrical And Surface Texture Characterization For Laser Powder Bed Fusion Process" (2023). *Open Access Theses & Dissertations*. 3936.
https://scholarworks.utep.edu/open_etd/3936

This is brought to you for free and open access by ScholarWorks@UTEP. It has been accepted for inclusion in Open Access Theses & Dissertations by an authorized administrator of ScholarWorks@UTEP. For more information, please contact lweber@utep.edu.

GEOMETRICAL AND SURFACE TEXTURE CHARACTERIZATION FOR LASER POWDER BED FUSION PROCESS

JESUS ALFREDO RIVAS ESCARCEGA
Doctoral Program in Mechanical Engineering

APPROVED:

Amit Lopes, Ph.D., Chair

Ryan Wicker, Ph.D.

David Espalin, Ph.D.

Vivek Tandon, Ph.D.

Stephen L. Crites, Jr., Ph.D.
Dean of the Graduate School

Copyright 2023 Jesus Alfredo Rivas Escarcega

GEOMETRICAL AND SURFACE TEXTURE CHARACTERIZATION FOR LASER POWDER BED FUSION PROCESS

by

JESUS ALFREDO RIVAS ESCARCEGA

DISSERTATION

Presented to the Faculty of the Graduate School of

The University of Texas at El Paso

in Partial Fulfillment

of the Requirements

for the Degree of

DOCTOR OF PHILOSOPHY

Department of Aerospace and Mechanical Engineering

THE UNIVERSITY OF TEXAS AT EL PASO

August 2023

ACKNOWLEDGEMENTS

I am ever grateful to my advisor and mentor Dr. Amit Lopes, for his guidance and support throughout this journey. Additionally, this research would not have been possible if not for the amazing resources at the W.M. Keck Center for 3D Innovation (Keck Center) but especially to all students, staff, and faculty that help me with a variety of experiments and assistance during this research. I specially acknowledge to Dr. Hunter Taylor for his valuable feedback, and support for experiments. I would also like to thank Dr. Wicker and the committee members Dr. David Espalin and Dr. Vivek Tandon for their knowledge, and constructive comments.

The research described here was performed at The University of Texas at El Paso (UTEP) within the W.M. Keck Center for 3D Innovation (Keck Center). This material is based on research sponsored by, in part, the Air Force Research Laboratory (AFRL) under agreement number FA8650-20-2-5700; award 70NANB21H006 from the U.S. Department of Commerce, National Institute of Standards and Technology (NIST). Additional support was provided by strategic investments via discretionary UTEP Keck Center funds, and the Mr. and Mrs. MacIntosh Murchison Chair I in Engineering Endowment at UTEP. The U.S. Government is authorized to reproduce and distribute reprints for Governmental purposes notwithstanding any copyright notation thereon. The views and conclusions contained herein are those of the authors and should not be interpreted as necessarily representing the official policies or endorsements, either expressed or implied, of AFRL, NIST or the U.S. Government.

ABSTRACT

Laser powder bed fusion (LPBF) is one of the most widely used additive manufacturing (AM) methods for metal parts. Geometrical tolerances required for industry applications are determined by geometrical measuring methods and process capability calculations. However, geometry characterization presents challenges for LPBF because measuring uncertainty values are not defined and the standardized measurement framework Geometric Tolerancing and Dimension (GD&T) is not fully adopted.

Measurement uncertainty is influenced by this process's high surface roughness (10 μm < Ra ⩽ 80 μm). As an example, when using multiple probing points or scanning pathways on a LPBF surface with the most accurate (+/- 0.004 mm) and traceable measurement method, the coordinate measuring machine (CMM), the results can vary by up to 0.050 mm to 0.070 mm. This measurement uncertainty leads to an imprecise benchmark reference for comparison with optical or X-ray computed tomography (XCT). These measurement variations also make it difficult to accurately characterize parts for automotive, aerospace, medical and other high-tech industries, such as a turbine blade geometry used in aircraft engines with a blade height tolerance of +/- 0.15 mm, which required a measurement uncertainty less than 30% of the tolerances. Mechanical properties such as tensile testing assessments useful in comparisons of materials, alloy development, quality control, and design under certain circumstances are also affected by this imprecise geometry characterization. Overestimating the diameter of the ASTM E8 sample by 0.100 mm can make up to a difference in stress results of 7%.

This research aimed to evaluate various measurement approaches (contact and non-contact) for surface texture and geometrical size dimension characterization and provide

information regarding measurement uncertainty and sampling procedures issues to accurately analyze the geometry and process capabilities needed for LPBF industrialization. Based on the research conducted, the LPBF's typical surface texture requires the definition of sampling procedures, and neither research nor industrial applications may directly use the manufacturer's declared repeatability and accuracy of a measurement method developed for the traditional manufacturing process.

To characterize a measurement system and improve the measurement process, statistical tools like the gage R&R (repeatability and reproducibility measurement assessment) are required. The first factor in choosing a measuring method is the tolerance range of interest. Fast and inexpensive measurement methods such as Micrometers and Calipers are an optimal solution when the measurement uncertainty range can be in a range of 0.100 mm. In contrast, Optical, and XCT measuring methods can achieve a medium measurement uncertainty range of 0.030 mm or less following a sampling procedure.

The results indicate that the surface of LPBF typically shows positive skewness and kurtosis values. This curve characterization can be used to estimate the percentages of geometrical deviations. A measurement framework based on a novel cross-sectional method, a combination of surface roughness measurements and size dimension measurements was proposed. The application of this work enables more precise geometric measurements used for research and industry assessments. Future research directions indicate the need for more measuring methods characterization and filtering approaches for asperities from attached particles, and partially melted particles to evaluate their contribution to mechanical behavior and geometrical form and fit properties.

TABLE OF CONTENTS

LIST OF TABLES

LIST OF FIGURES

CHAPTER 1: INTRODUCTION

BACKGROUND

The constraints imposed using conventional manufacturing processes are being changed by additive manufacturing (AM). New capabilities include the capacity to generate complex geometry, integrate various parts into one assembly, employ various materials during one production cycle, and shorten the time between the development of a prototype and the fabrication of a functional part.[1] The ISO ASTM 52900 2015[2] standard categorizes all AM processes into seven broad subclasses. Where Powder Bed Fusion is defined as follows:

Powder bed fusion, PBF: "an AM process in which thermal energy selectively fuses regions of a powder bed." This category contains the laser-based powder bed fusion process (L-PBF), and according to the ISO/ASTM standard, the process should be described as using a laser beam (LB) with the acronym PBF-LB in technical documentation. However, the terminology L-PBF is widely in use and is acceptable. This category also contains electron beam powder bed fusion (PBF-EB).

Laser powder bed fusion (LPBF) is a dominant technology in metal additive manufacturing processes and offers unique advantages such as the ability to fabricate complex internal geometric structures or the implementation of topology optimization for a broad range of industries including aerospace, energy, medical, and tooling. Although the idea behind the procedure is straightforward (adding material layer by layer following a 3D design), it becomes complicated since more than one hundred input parameters may have an impact on the quality of the finished part. These variables can be categorized into four primary groups (Machine-based, Material-based, Process

parameters, and Post-treatment parameters). Research is still ongoing to establish how altering some parameters will affect how they interact with one another.[3–6]

PROBLEM AND RESEARCH QUESTIONS

Traditional manufacturing methods typically use the term "process capabilities," which is defined as a process's ability to produce goods that meet predetermined specifications.[7] Geometrical measurement methods in conjunction with process capability calculations determine target values and geometrical tolerance. To enable broad industrial applications of AM parts, process capability indicators must be defined. However, when applied to laser powder bed fusion, measurement characterization with both contact and non-contact methods presents challenges because measuring uncertainty values are not defined, the standardized measurement framework Geometric Tolerancing and Dimension (GD&T) is not fully adopted, and sampling strategies are still being researched.[8,9]

Coordinate measurement machines (CMM) are the most accurate and traceable measurement methods. High-accuracy CNC coordinates measuring machines such as (CRYSTA-Apex S 500/700/900/1200 guarantees a maximum permissible error of (1.7+3L/1000 μm) when L refers to sampling length.[10] This measuring method is used as a benchmark reference to compare against Optical or X-ray Computed Tomography (XCT) for additive manufacturing sample evaluations.[11–13] The measurement uncertainty for LPBF is shown to be influenced by the high amount of surface roughness (10 μm < Ra ⩽ 80 μm).[14,15] For instance, when using multiple probing points or scanning pathways on the same surface with the most accurate and traceable measurement method (CMM), the results can vary by up to 50 μm to 70 μm, which makes it difficult to accurately characterize a geometry.[16]

Implementing standardized measurement frameworks like the American Society of Mechanical Engineers (ASME) Y14.5 2009 or International Organization for Standardization (ISO) 1101 are needed to fully characterize the capabilities of the process, rather than depending exclusively on the printing resolution and minimum feature size specified by the machine manufacturer. High-tech parts in the aerospace or aircraft industry with a special interest in LPBF have small tolerances such as turbine blade geometry used in aircraft engines with a blade height tolerance range of +/- 0.15 mm or less. These tolerance values require optimal geometrical and surface characterization. Analysis of measuring systems has been used to assess measurement accuracy and identify the causes of measuring errors. Methodologies such as "Gauge R&R" Reproducibility and Repeatability analyze the measuring variance caused by different measurement configurations, such as equipment or operators, as well as the variation under the same sample settings. According to this method, a measurement error contribution to the final tolerance in the range of 30 % or less is acceptable. Based on the turbine blade example, a measuring error of less than 0.050 mm is necessary to assure that the part is functional, but several measurement frameworks for LPBF do not allow for this precision to be achieved.[17] Measurement techniques and surface characterization raise several research questions, including:

- What measuring system evaluation procedure should be used to guarantee accurate geometries characterization for LPBF?
- What measurement technique is ideal for LPBF parts?
- What accuracy and precision constraints must be considered to validate the geometrical tolerances and LPBF process capabilities?
- What factors are crucial for LPBF surface texture characterization?

SIGNIFICANCE OF THE RESEARCH AND ORGANIZATION

To accurately analyze the process capabilities of LPBF, this research enhanced measurement system procedures and considerations. This research assessed several measuring approaches (contact and non-contact) for surface texture and geometrical size dimension characterization and provided details regarding measurement uncertainty and sampling procedure issues. The dissertation is organized as follows, Chapter 2 provides a literature review for additive manufacturing geometrical characterization, measurement systems for laser powder bed fusion, and surface texture characterization. Chapter 3 describes the materials and methods used to address the research questions. Chapter 4 shows the results obtained from the data collection. Chapter 5 Conclusions and Discussion.

CHAPTER 2: LITERATURE REVIEW

This chapter provides a survey of the literature on the geometrical characterization of laser powder bed fusion to describe its accuracy and precision. The measurement systems employed for the characterization of contact and non-contact approaches are reviewed in the subsections. Due to the significance of tolerance capabilities for industry applications, the Geometrical Dimensional and Tolerancing (GD&T) standard used for conventional manufacturing processes is also assessed. Finally, the chapter discusses the technique used to characterize the surface texture and its correlation with the measurement systems.

LASER POWDER BED FUSION GEOMETRIC CHARACTERIZATION

Laser Powder Bed Fusion (LPBF) is capable of producing metal parts with unique geometries and complex internal structures for automotive, aerospace, medical, and other high-tech industries.[1] Nevertheless, the implementation of the LPBF process presents challenges in terms of qualification and certification with standards and procedures for metal AM not fully defined or adopted.[18] In the aim of expanding industry applications for LPBF, manufacturing tolerance (process capabilities) and tolerance verification (measurement uncertainty) needs to be clearly understood and defined.[19] Influence factors of the LPBF process, that have an impact on geometrical tolerances can be categorized into four large groups (Machine-based, Material-based, Process parameters, and Post treat parameters). The main process parameters related to geometry deviation are laser power, scan speed, hatching speed, hatching distance, scanning strategy, beam offset, and scaling factor.[20]

Dimensional accuracy is fundamental to ensure proper mechanical assemblability and functionality based on geometrical design specifications. The conventional accuracy range for LPBF can be estimated with about 100 µm dimensional deviation.[21] Several authors have evaluated parts accuracy based on different process parameters, materials, and types of geometries.[20,22] In an attempt to qualify the accuracy of metal additive manufacturing a Geometric Dimensioning and Tolerances (GD&T) framework has been used to define geometric characteristics such as cylindricity, angularity, and concentricity tolerances produced on benchmark test artifacts (GBTAs).[9,23–28] As an example, the Global Test Artifact Data Exchange Program (GTADExP:https://gtadexp.org), a program managed by the W. M. Keck Center for 3D Innovation at the University of Texas at El Paso by Taylor et al. (2021) intends to accelerate the holistic understanding of metal laser powder bed fusion using a comprehensive artifact shown in Figure 1.[29]

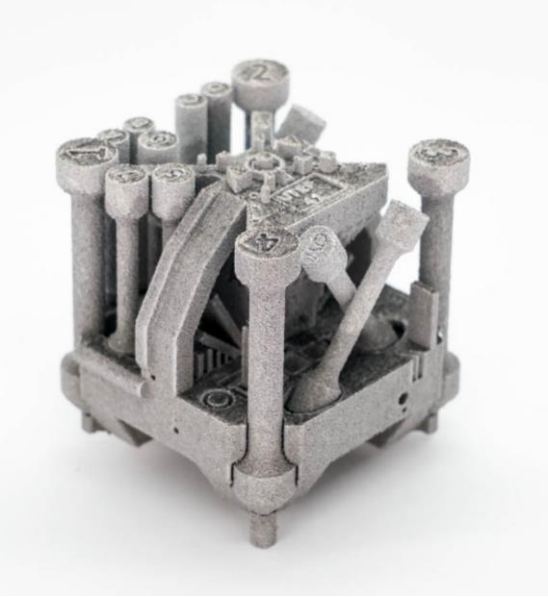

Figure 1 Global test artifact.

Very few geometric benchmark testing artifacts provide information using a complete GD&T analysis. Tolerances like profile, surface, and true position are among the characteristics rarely considered in existing GBTAs. Multiple identical features present in GBTAs evaluate the system capabilities to produce the feature at various locations but do not evaluate process repeatability. Yang *et al*. (2014) proposed a minimum set of geometrical features with various dimensional scales to reduce feature design redundancy with a matrix between GD&T characteristics and the underlying process characteristics and determined that thermal profile and gravity have a compound effect on the overall shape and individual geometric characteristics such as flatness and cylindricity.[30] The importance of the measurability of an artifact is highlighted in several studies because it affects the design process of the artifact and the measurement method.[9]

Weaver *et al*. (2017) compared the expected accuracy and precision of AM process and classified LPBF with a range from 75 µm to 200 µm in contrast with traditional manufacturing subtractive processes such as large boring or small milling with values below 0.025 µm.[31] Gradl *et al*. (2021) reported a systematic error mean for build accuracy of 23.8 µm across different types of features with upper and lower control limits of +220 µm / - 260 µm on standardized ISO/ASTM test artifact on Inconel 718 material.[32] Kozhuthala *et al*. (2021) evaluated the effect of the sample's position on the build plate with respect to the shrinkage and dimensional deviation and found more deviation in the perpendicular direction of the gas flow than in parallel for a circular shape and samples printed close to the gas nozzle, where these variations were related to differences in the cooling rate and pressure of assisted gas.[33]

To estimate the tolerance capabilities, diverse geometry configurations should be considered, such as part build orientation which is related to geometry quality errors. Various models have been developed to optimize the part build orientation and support structural[30,34,35]

Tolerance capabilities based on benchmark evaluation are limited due to the range of feature orientations produced.[36] Some authors have developed methods to compensate and predict geometrical deviation. Afazov *et al*. (2017) proposed an approach for modeling the induced distortion of the LPBF process and compensating by using Finite Element Analysis (FEA) distortion and Optical 3D scan measurements.[37] Tolerance estimation and control require a correct measurement method selection and measurement procedure definition when evaluating AM metal parts. Mahshid *et al*. (2018) performed a tolerances analysis using process capabilities and measurement uncertainty and found a significant reduction in the conformance zone due to measurement errors.[15]

LPBF CALIBRATION BASED ON MEASUREMENT RESULTS

The scaling factor is used to account for the thermal expansion during the build and subsequent shrinkage post-build. Since the builds are typically done with a heated build plate and the process of laser melting adds heat to the system, the parts are in an expanded state during LPBF processing and will shrink after the build is complete. To account for this shrinkage, a scaling factor can be used to increase the size of the part before slicing. The magnitude of error induced by shrinkage is expected to match the materials coefficient of thermal expansion however the error could also be due to the laser scanner calibration which is typically done by the equipment manufacturing during preventative maintenance. Calibration error is unlikely to be linear and symmetric in both X and Y directions as the calibration accounts for pillow and barrel deviation.[38] The primary parameters to improve surface integrity and fine feature detail are the contour scans since they serve to reduce roughness and potentially increase dimensional accuracy by smoothing the start/end of interior hatching vectors as observed in detail in the laser scanning offsets in Figure

2. The programmed contour parameters assume a zero-width line, though in actuality, the laser beam and the melt pool have a two-dimensional (2D) width. Hence, it is important to offset the scanning position of the contour to account for this melt pool width. This offset is usually referred to as the global offset and some LPBF equipment manufacturers refer to this offset as beam compensation. The global offset must be set according to the contour power and speed as these parameters directly affect the melt pool width. An error in the prescribed contour offsets and beam compensation should be consistent across all features in the artifact. For example, if the global offset is too large then all cylinder protrusions should be undersized by a constant value and not vary with cylinder diameter.[39]

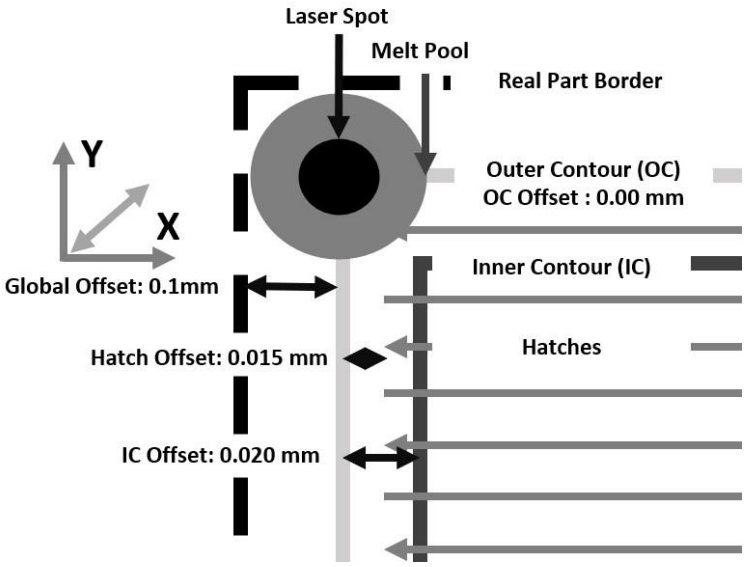

Figure 2 Scanning offset parameters.

MEASUREMENT SYSTEMS FOR LASER POWDER BED FUSION

As stated in the Evaluation of measurement data — Guide to the Expression of Uncertainty in Measurement:[40]

When reporting the result of a measurement of a physical quantity, it is obligatory that some quantitative indication of the quality of the result be given so that those who use it can assess its reliability. Without such an indication, measurement results cannot be compared, either among themselves or with reference values given in a specification or standard.

Two of the most common statistical properties used to characterize the quality of measurement data are **bias** and **variance**. The term **bias** is related to the location of the average measurement data relative to a reference value, where **variance** is related to the spread of the data.[41] Accuracy is a qualitative term used to specify the closeness to the true value, where precision is the closeness of the repeated reading to each other. For any measurement report, it is important to indicate the quality of the measurement results, so the use of the data is reliable. Measurement uncertainty: according to the Guide to Expression of Uncertainty (GUM) is defined as:

"Parameter, associated with the result of a measurement, that characterizes the dispersion of the values that cloud reasonably be attributed to the measurand."

A measurement uncertainty assessment consists of identifying and quantifying all sources of measurement errors. Methods for evaluating uncertainty include statistical approaches when a

series of repetitions can quantify the precision of the measurement system to provide the same result under the same configurations. Other sources of measurement uncertainty such as calibration certificates, or measurement device resolution are included as well. The guide to the expression of uncertainty used the term "**Type A**" and "**Type B**" to categorize the source of uncertainty. Equation 1 shows a **Type A** uncertainty calculation based on the standard deviation formula for measurement repeatability evaluation where **x** is the measurement value a $\bar{x}$ is equal to the sample mean and **n** is the number of repetitions. In contrast, equation 2 shows a **Type B** evaluation where the stated accuracy a from the reference manual of the equipment is used for the overall measurement uncertainty calculation. The term "$\mathbf{u_C}$" is used to express the combined uncertainty according to equation 3 with all identified uncertainty contributors either **Type A** or **Type B**. The term "**U"** is the combined uncertainty times the coverage value "**K**" which is related to the number of degrees of freedom to express a confidence interval of 95%.

Equation 1 Type A $u_1 = \sqrt{\frac{\sum(x-\bar{x})^2}{n-1}}$

Equation 2 Type B $u_2 = \frac{a}{\sqrt{3}}$

Equation 3 $\mathbf{u_C} = \sqrt{\mathbf{u_1^2 + u_2^2 + u_3^2 + u_4^2}}$ $\mathbf{U = Ku_C}$

CONTACT MEASUREMENT METHODS (CMM, MICROMETER, CALIPER)

Measurement methods can be categorized as contact and non-contact. The contact measurement method coordinate measuring machine (CMM) is considered to have the best accuracy and traceability with a range of accuracy of 0.004 mm or less. This method is utilized as a benchmark against contact and non-contact devices and less accurate methods such as XCT or Optical. Several studies have evaluated AM parts around different measurement systems approaches, however, high surface roughness values on additive manufacturing parts have been proven to not only affect the mechanical functionality but the measurement results. Lou *et al*. (2019) investigated the mechanical filtering effect on tactile measurements of additive manufacturing parts and found a relationship between the maximum measurement error caused by the stylus mechanical filtering effect and the convex hull points of the measurement profile.[42]

A specific type of geometry with measurement challenges are the lattice structures, commonly used in aerospace and medical applications. The standard ASME 14.46[43] developed for AM suggests the use of theoretical supplement surfaces for each lattice connection definition. Praniewicz *et al*. (2020) studied the sampling location and their relationship with the topology surface variation under this approach. They highlighted the measurement variation in terms of sampling location.[12] Berez *et al*. (2014) evaluated different probing points or scanning paths used in CMM with results in different surface samples with up to 0.050 mm to 0.070 mm variations in some cases.[16]

According to the CMM Good Practice Guide[44], the general measurement strategy for CMM include:

1. Selection of the features on the workpiece to be measured.

2. Definition of the workpiece datum feature(s) to be used within the co-ordinate system.

3. Selection of the workpiece orientation.

4. Selection of the workpiece holding method.

5. Stylus system qualification.

6. Definition of the probing strategy.

7. Programming of the CMM and assessment information recording.

Calipers are versatile measuring tools able to measure several types of dimensions such as inside dimensions, outside dimensions, depth, and step height.[45] The maximum permissible error (MPE) is the specified limit value for measurement errors. High-resolution 0.01 mm calipers have +/-0.02 mm of MPE for a measurement length from 0 mm to 50 mm. As the length increases from 50 mm to 100 mm the MPE increases to +/- 0.03 mm.

A variety of types of micrometers exist according to different measurement applications. Such as inside micrometers, depth micrometers, and outside micrometers. The measurable range differs every 25 mm—such as 0 mm to 25 mm and 25 to 50 mm depending on the size of the frame, so using a micrometer that matches the target size is necessary. A Maximum Permissible Error (MPE) of +/- 0.004 mm for length measurement in a range of 0mm to 25mm is expected with these devices.

NON-CONTACT MEASUREMENT METHODS (XCT, OPTICAL)

XCT is a promising nondestructive evaluation method for AM part characterization due to its unique ability to measure internal features and defects.[46] However, XCT is not a mature technology in comparison with conventional tactile Coordinate Measuring Machines (CMM) for dimensional metrology.[13] The quantification of uncertainty of Computed Tomography (CT)

dimensional measurements is a complex problem for the error sources involved and the lack of an accepted model of a comprehensive measurement process and standard procedures.[47] Carmignato *et al*. (2017) studied the effect of surface roughness and acquisition image parameters in dimensional measurement for XCT, where smaller measurement values than CMM reference measurement were obtained with a relationship approximately 2Rp (maximum peak height of the profile in the sampling length), on average.[48] A systematic error between XCT and CMM measurements about Rz (referred to as the maximum roughness) parameters from 30 μm to 125 μm can be estimated. For example, external diameters are smaller than CMM approx. Rz/2 and internal diameters are bigger than CMM with Rz/2. Villarraga (2018) evaluated the differences between CMM and XCT on non-additive manufacturing parts, range differences of approximately 5 μm to 50 μm were found in 0.5 mm to 65 mm sizes features at optimized conditions.[49]

Optical measurements exhibit finer resolutions than XCT and have gained relevance due to the rapid verification of AM parts in combination with geometrical dimensioning and tolerancing.[12] This method has comparatively lower cost and ease of use than CMM and XCT, and it is more widely adopted for in-line inspection of production parts, across a variety of industries Giganto *et al*. (2020) evaluated different Optical measurement systems based on different sensors and working principles and identified portable systems handheld laser triangulation and structured blue light scanners as the most accurate Optical options for scanning LPBF parts.[50] A similar investigation determined laser triangulation and structured light as optimal on rough surfaces produced on AM parts.[51] The effect of high surface roughness and large numbers of slopes and loose particles have been studied with different sampling techniques such as coherence scanning

interferometry where the surface characteristics challenge the accurate measure of surface topography at high resolution.[52]

GEOMETRIC DIMENSIONING AND TOLERANCING (GD&T) AND SIZE DIMENSION

The adoption of AM in the industry has significant barriers related to the prediction and evaluation of the output geometry before and after printing the part. Factors such as part size, materials cost, part quantities, and other time and financial constraints all contribute to the importance of process prediction and evaluation. Using manufacturer-reported printing resolution and minimum feature size is not sufficient to ensure geometric functionality in industry applications. Feature location and orientation tolerances are needed to ensure assembly among parts. Geometric dimensioning and tolerancing (GD&T) provide a framework for evaluation in terms of geometric functionality and inspection of production parts based on standards such as American Society of Mechanical Engineers (ASME) Y14.5 2009[53] or International Organization for Standardization (ISO) 1101:2012.[54]

GD&T is based on four fundamental controls (size, form, orientation, and location) to geometrically describe a feature. How big is the feature? (size), What is the shape of the feature? (form), How is the feature located and oriented? (To ensure assemblability or functionality) as shown in Figure 3.

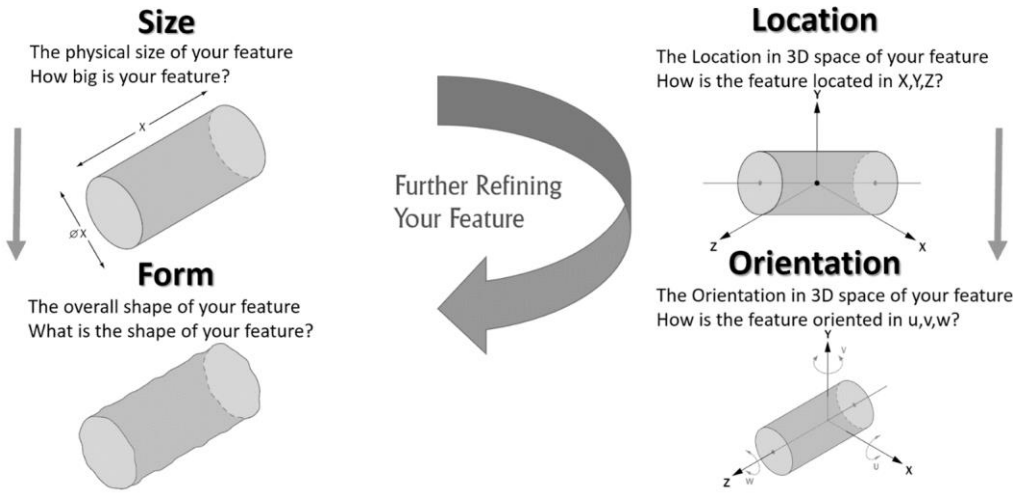

Figure 3 Fundamentals controls (size, form, orientation, and location) to geometrically describe a feature.

A datum reference frame is used to define the orientation and location of the feature of interest based on planes, axis, or points of reference. The geometric characteristics can be categorized in form, profile, orientation, location, and runout with induvial characteristics used according to the application.

- **Form** Straightness, Flatness, Circularity, and Cylindricity.
- **Profile**. -Profile of a line, Profile of a surface.
- **Orientation**. - Angularity, Perpendicularity, Parallelism
- **Location**. - True position, Concentricity, Symmetry
- **Runout**. -Circularity, Runout, Total runout.

Size dimension

ISO 14405 is the geometrical product specification (GPS) standard for linear sizes and defines special modifiers for features of size. Figure 4 shows the size variation based on different global size ISO 14405 approaches, maximum inscribed size, and minimum circumscribed size. The variation is expected to be proportional to the surface's roughness. [55] Figure 4 shows the size variation on a cross-sectional circular geometry produced with LPBF and different global size approaches maximum inscribed size and minimum circumscribed size. Since the surface roughness of LPBF is expected to be higher than traditional manufacturing methods, the variation in reported size based on the size approach will be higher.

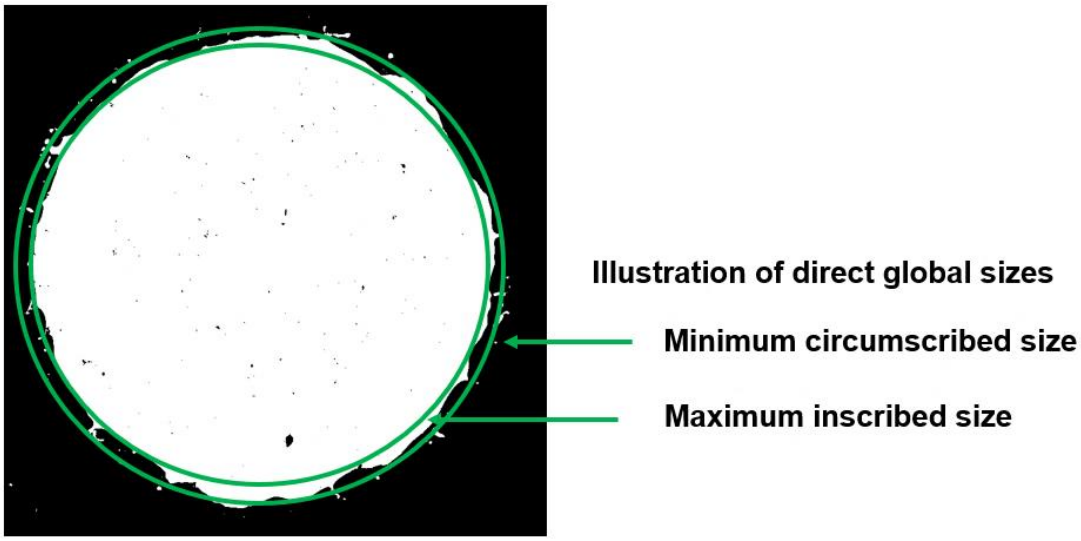

Figure 4 Size variation based on different global size approaches of a circular geometry produced by LPBF.

Figure 5 shows a measurement diameter of an LPBF part made of AT grade 5 Ti-6AL-4V with a surface roughness Sa=0.011 mm, the diameters variations based on maximum inscribed size and minimum circumscribed size are observed (2.062 mm versus 1.812 mm). These differences increase the measurement uncertainty to determine the true diameter size.

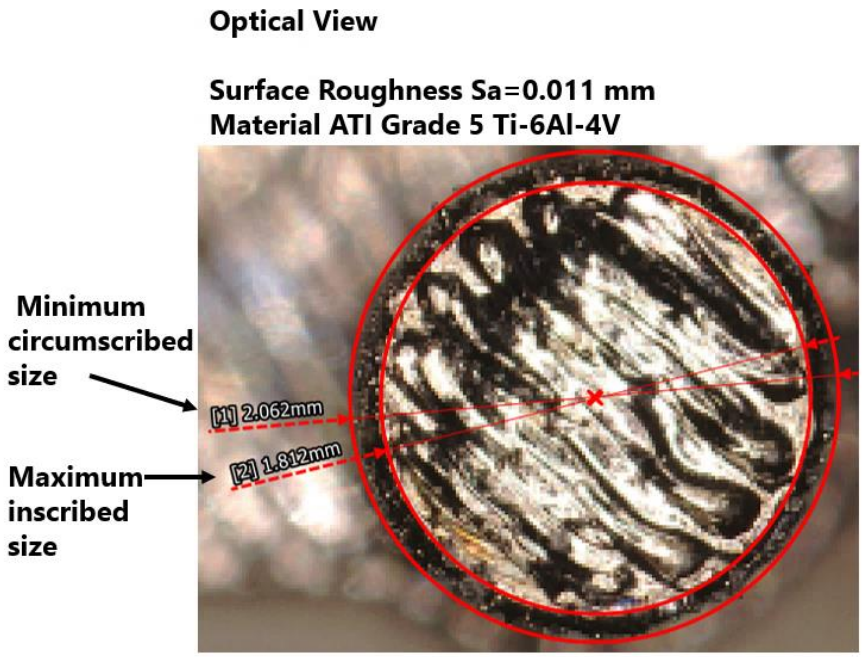

Figure 5 Measurement diameter of LPBF part made of AT grade 5 Ti-6AL-4V.

SURFACE TEXTURE CHARACTERIZATION

The American National Standards Institute (ANSI) defines surface texture as:

"The repetitive or random deviation from the nominal surface that forms the three-dimensional topography of the surface ... including roughness, waviness, lay, and flaws." [56]

Surface texture can be separated based on the variation at different scales, such as short wavelength roughness, waviness, and form at intermediate and longer wavelengths. Methodology for

extraction of maximum peak to valley height (Rz), and arithmetical mean deviation, (Ra) are shown for a given assessment length in Figure 6.

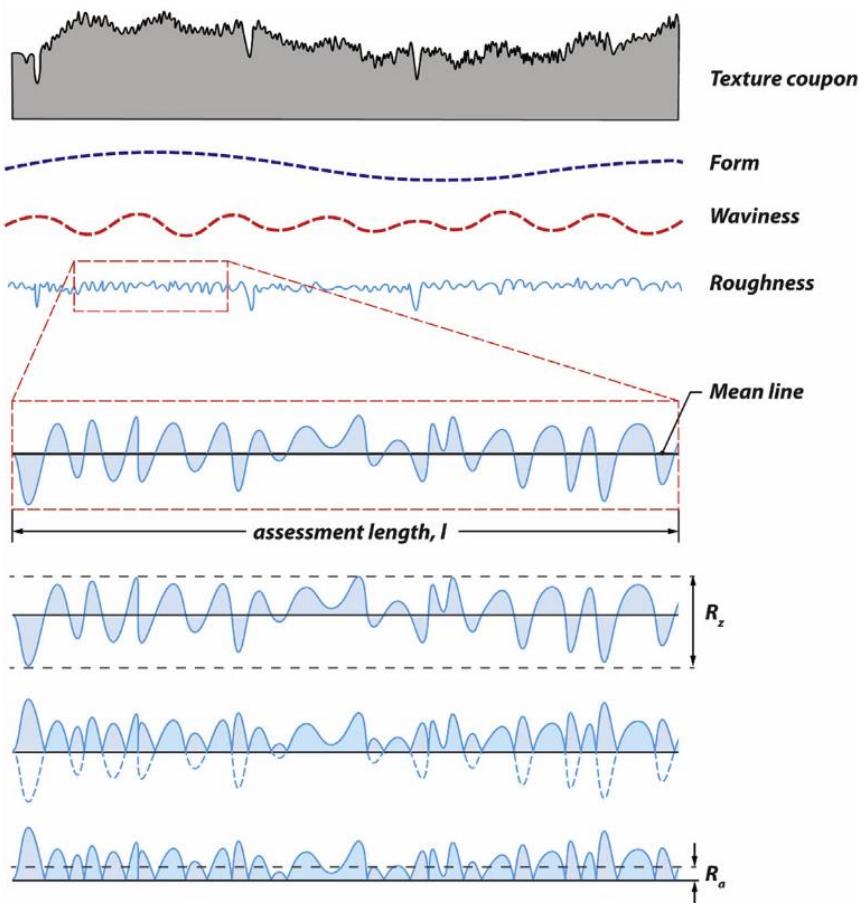

Figure 6 Surface texture at different scales (Whitehouse, D.J., 2002. Surfaces and Their Measurement. HPS, London).

Several standardized surface texture parameters are defined to represent different characteristics as defined by the following equations:

Arithmetical mean height indicates the average of the absolute value along the sampling length and is defined by equation 4. Where ***Z*** *is the height of the irregularities,* ***x*** *is the sampling*

length and ***Ir*** *is the interval or filter used and the nomenclature (P) profile, (R) roughness, and (W) Waviness*.

Equation 4

$$Pa, Ra, Wa, \frac{1}{I_r}\int_0^{Ir} |Z(x)| \, dx$$

Maximum profile peak height indicates the point along the sampling length at which the curve is highest defined by:

Equation 5

$$Rp = |\max(Z(x))|$$

Maximum profile valley deep indicates the point along the sampling length at which the profile curve is the lowest defined by:

Equation 6

$$Rv = |\min(Z(x))|$$

The maximum height of the profile indicates the absolute vertical distance between the maximum profile peak height and the maximum profile valley deep along the sampling length defined by:

Equation 7

$$Rz = Rp + Rv$$

Root means square deviation indicates the root mean square along the sampling length defined by:

Equation 8

$$Pa, Ra, Wa = \sqrt{\frac{1}{Ir}\int_0^{Ir} Z^2(x) \, dx}$$

The surface roughness on LPBF is significantly higher than in the traditional manufacturing process. Several parameters from preprocess, process, and post-process influence the final surface texture. It is observed, for example, the variation based on the inclination angle about the print bed. The importance of understanding the final surface texture is fundamental to understanding the mechanical behavior and geometrical form and fit properties of the LPBF-produced parts.[57]

The surface texture variation underlying reasons can be categorized as follow:

- Stair–step effects Layer thickness and component inclination angle.
- Spattering of satellite particles from the ejection of particles from the melting pool and neighboring regions.
- Stability of the melt pool and associated morphology of the solidified laser track resulting in nonuniform of the track geometry.
- Melt pool phenomena vapor pressure, internal convection currents, and surface tension.
- Contact with the powder bed during the melt pool solidification on surfaces that are not upward-facing.
- Neighboring tracks interaction especially in complex local geometry.

Where these roughness phenomena are influenced by design variables including:

Pre-process parameters: Powder size, particle distribution, build plate preheating chamber environment.

Process parameters: Scanning speed, laser power hatching spacing, layer thickness, scanning strategy.

Post-process parameters: Heat treatment, material removal process.

The selection of appropriate cut-off wavelength, evaluation length, and measurement area represents a challenge in additive manufacturing. Random asperities across the surface related to the parameters described produced significant variation in the results. Nagalingam *et al*. (2021) investigated a framework of surface texture characterization based on the asperity's diameters and waviness cut-off wavelength filter value, with the suggestion of the use of 2.5 times the maximum asperities size as the value for cut-off wavelength filter and compromise the sampling length for small sections.[58] Townsend *et al*. (2016) reviewed surface metrology in terms of the additive manufacturing process domain, and highlighted the presence of asperities from attached particles, partially melted particles, or asperities related to the staircase effect as factors to consider for surface texture characterization.[59]

When evaluating LPBF specimens, macro geometry errors can be categorized as (Form) and are related to nominal geometry deviation due to thermally induced residual stress. In contrast, a point between macro and micro is categorized as (Waviness) and occurs at the local resolution, for example, due to the stair-set effect. Finally, micro-scale errors (Roughness) can be associated with individually adhered particles and irregularities.[57] Adopting standardized measurement procedures ISO 4288 for profile and ISO 25178-2 for areal surface texture are not well defined for AM.[58] Arithmetic mean value Ra (average of the absolute values of the profile height deviations from the mean line) is the most widely used by traditional manufacturing methods. However, the sensitivity to reporting the typical outliers found in AM in the form of peaks and valleys is limited. It has been documented that significantly different surfaces have the same Ra value. Based on the ISO 4288 in Table 1 a measuring length (ln) of 40 mm with a cut-off wavelength filter length (λc)

of 8mm is recommended for the expected metallic additively manufacturing parts of 10 μm < Ra ⩽ 80 μm. However, this measuring length is not practical in typical sample sizes.

Table 1 Cut-off wavelength filter values according to ISO 4288-1996.

Cut-Off values according to ISO 4288-1996			
Non-periodical profile		**Cut-Off**	**Basic length of roughness/ Evaluation length**
Rz (μm)	Ra (μm)	λc (mm)	lr/ln (mm)
to 0.1	to 0.02	0.08	0.08/0.4
>0.1 to 0.5	>0.02 to 0.1	0.25	0.25/1.25
>0.5 to 10	>0.1 to 2	0.8	0.8/4
>10 to 50	>2 to 10	2.5	2.5/12.5
>50	>10	8	8/40

Sampling parameters such as measuring length (ln) and cut-off wavelength filter length (λc) have a significant effect on the results and are still under research. Different standardized cut-off wavelength filter lengths (λc) 0.08 mm, 0.25 mm, 0.8 mm, and 2.5 mm for the same surface can have a variation in a range of 20 μm for Ra parameter.[60]

Chapter 2 presented a literature review related to the research questions proposed in Chapter 1. The following conclusions can be drawn about qualifying the process and measurement. Printing parameters: Laser powder, scan speed, hatching distance, or scanning strategy have been identified by several authors as influential factors that have an impact on the geometrical tolerances. Dimension accuracy is fundamental to ensure proper mechanical assemblability and functionality for expanding LPBF in industry applications. The accuracy qualification of metal additive manufacturing based on the standardized geometrical dimension and tolerancing (GD&T) is still under research. Statistical methods and standards such as GUM to analyze measurement systems are required to characterize the quality of a measurement. The high surface roughness values on additive manufacturing parts affect not only the mechanical functionality but the measurement results. Novel approaches to correlate measurement uncertainty and surface texture parameters are needed to better characterize the measurement results. The adoption of standardized surface roughness characterization as ISO 42884 profile or ISO 25178-2 for surface area for AM and still under research. Sampling parameters such as cut-off wavelength filter and evaluation length effect on the reported value are not well defined for AM.

CHAPTER 3: MATERIAL AND METHODS

Chapter 3 presents the Materials and Methods used to address the research questions presented in Chapter 1. The purpose of the dissertation is to contribute to the process and measurement capabilities definition needed for increasing LPBF applications in the industry. Based on the literature review, the qualification of measurement systems is still under research as well as the effect of the high level of surface roughness for systems characterization and tolerancing. The chapter is organized as follows; Material (contact and non-contact, qualification test Artifact) and Methods (repeatability and reproducibility of a measurement system evaluation, comparison of contact and non-contact measurement systems, surface texture characterization).

MATERIALS

Contact and non-contact measurement

The following section presents the contact and non-contact methods used for the dissertation work. The investigated measurement techniques provide a complete range of methodologies with different investments in terms of capital (XCT~$1,000,000, CMM ~$500,000, Caliper and Micrometer ~ 500, Optical~$100,000) and training (XCT~months, CMM ~weeks, Optical~days, Caliper and Micrometer ~ hours).

Coordinate-Measuring Machine (CMM)

CMM measurement was performed on a Zeiss Prismo, serial number 115281 (Carl Zeiss AG, Oberkochen, Germany) by an external Inspection Engineering laboratory and certified that all measurements comply with ISO/IEC 17025 and/or to NIST (National Institute of Standards and Technology) in accordance with MIL-STD 45622A with a reported uncertainty ±2.5 µm, Laboratory temperature 20.9˚C and 48.1% relative humidity. Six different probe tips were used for the complete artifact evaluation with a 0.20 mm diameter stylus for difficult-to-access features.

Caliper and Micrometer

Digital Caliper (iGAGING, Los Angeles, California) with a range of 0-6 inches, model 100-333-8 was used for all applicable feature types (Figure 7), had a reported accuracy of 25 µm, repeatability of 12 µm, and a resolution of 10 µm. Micrometer (Mitutoyo) model 293-831-30, with a reported accuracy of 2.5 µm, resolution of 10 µm obtained for the manufacture report manual, and a flat measuring face with a 6.35 mm diameter size was used to determine the diameter sampling bar dimensions.

Figure 7 Feature measured by the micrometer method.

Optical

A Keyence VR-5200 (Keyence Corporation, Osaka, Japan) wide-area three-dimensional (3D) measurement system was used for the Optical method. 2D plane measurement tools as observed in Figure 8 with a reported high magnification of 40x (high resolution), tolerance of 0.5 µm for repeatability, and measurement accuracy of ±2 µm.[61]

Figure 8 2D Plane measurement by an optical method.

X-ray Computed Tomography (XCT)

XCT datasets were acquired with a Pinnacle PXS-225/70 (Pinnacle X-Ray Solutions Inc., Georgia, United States), characterized by a micro-focus X-ray source with a tungsten target. A total of 1440 radiograph projections over 360° rotation were captured by a Varex XRD 4343CT Flat Panel detector with 2880 X 2880 pixels. Each artifact was positioned inside the XCT at a 45° tilt using a fixture. A fil-projection (FBP) algorithm with a ramp noise suppression filter was used

within the CT reconstruction module of VGstudio Max 3.5 software (Volume Graphics, GmbH, Heidelberg, Germany); additional parameters are summarized in Table 2. VGstudio MAX 3.5 software was used to determine the surface of the reconstructed volume. The Gaussian least-squares fitting process was used for the creation of geometrical elements (e.g., planes) with the auto-expansion of points with a search distance equal to 0.07 mm, step width of 0.017 mm, and a maximum number of points of 1000 as observed in Figure 9.

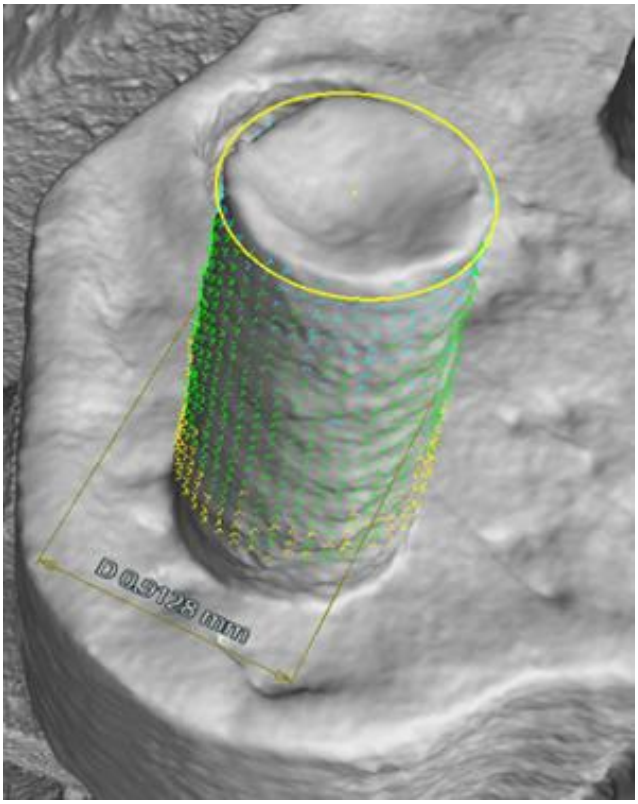

Figure 9 Pin from Qualification Test Artifact (QTA) measurement example by XCT method.

Table 2 Sampling parameters.

Parameter	Value	Units
Voltage	225	Kv
Current	190	mA
No. projections	1440	-
Exposure time	1000	ms
frames per projection	4	images
Pre-filter Cu	1	mm
Voxel size	0.0189	mm

Qualification Test Artifact (QTA)

The sampling geometry used for this study is part of the Qualification Test Artifact (QTA) from the Global Test Artifact Data Exchange Program (GTADExP) – a program designed to advance knowledge in metals LPBF fabrication capabilities in support of broadening adoption of the technology.[29] Figure 10 illustrates the overall design of the artifact and includes a set of basic geometries such as cylinders, holes, rectangular recessions, and extrusions selected for geometry evaluations. Three versions of the artifact were used for this dissertation, some geometrical changes were based on the preliminary result of this work. The QTA is designed to be a compact but comprehensive test artifact from which data for analysis of the chemical composition, microstructure, surface integrity, residual stress, mechanical properties, and more may be gathered.[62] Additionally, the QTA has many features specifically designed to test the geometric accuracy of the various features.

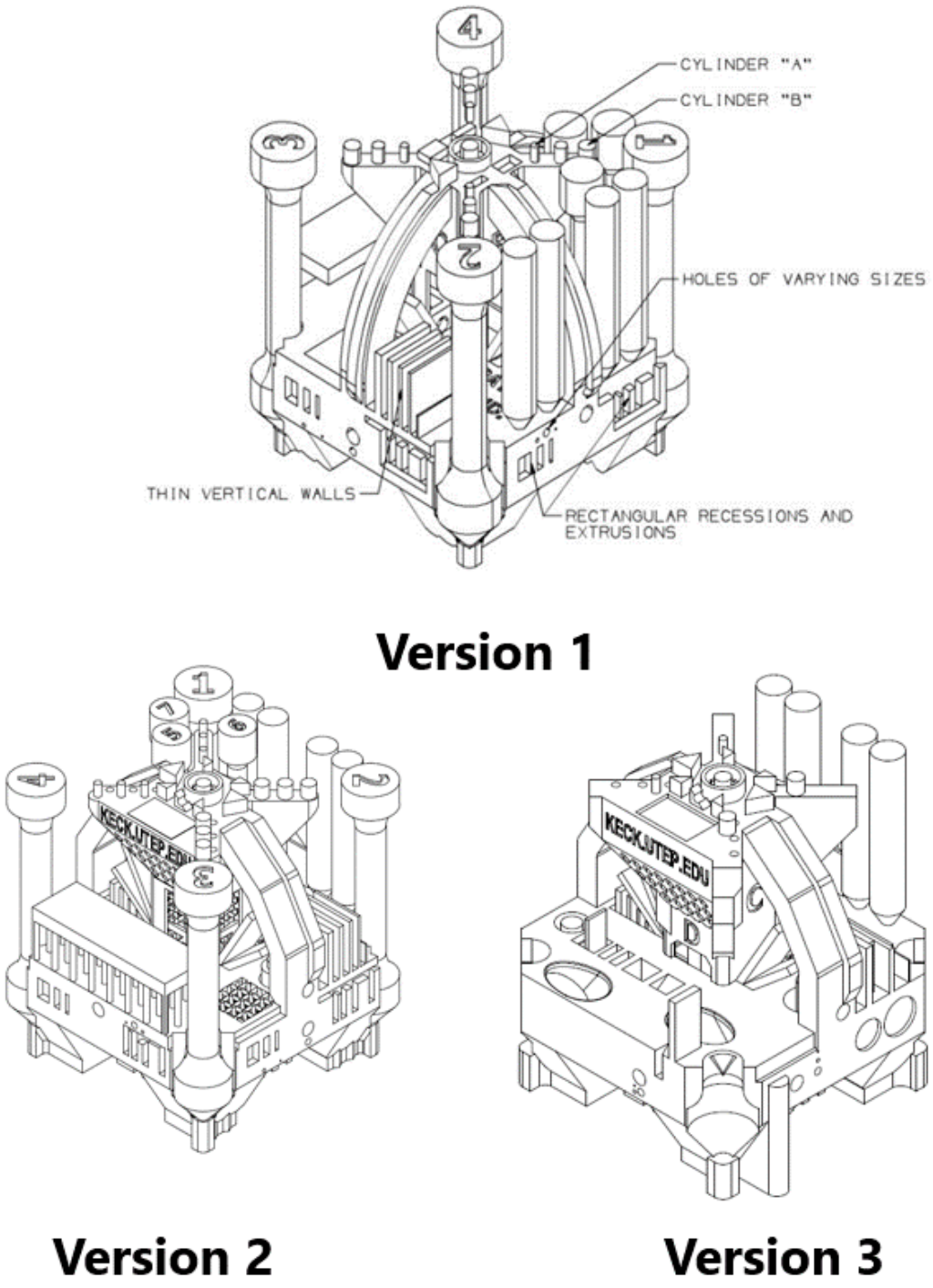

Figure 10 Qualification Test Artifact (QTA) versions from the Global Test Artifact Data Exchange Program (GTADExP).

METHODS

Repeatability and reproducibility of a measurement system

For this study, a non-contact Optical measurement system was selected over a coordinate-measurement machine (CMM) and X-ray Computed Tomography (XCT). A key driver in the choice of a non-contact image-based measurement system is the balance between speed, accuracy, and cost. This measuring method is commonly used in line production for traditional manufacturing processes. This study evaluated the measuring repeatability and reproducibility when it is applied to Laser Powder Bed Fusion samples. The result contributed to the research question, *what measuring system evaluation procedure should be used to guarantee accurate geometries characterization for LPBF?*

A gage R&R study was performed to verify the measurement capabilities of the system. Five samples of artifact version 1 were printed, and all measurements and tolerances followed the ASME GD&T Y14.5 standard. The results from the data analysis helped to determine the variation between the manufacturer's stated accuracy and repeatability and the variation when applied to LPBF.

Test artifact print parameters

All builds used in the study were performed on an EOS M290 (EOS GmbH, Germany) with ATI Grade 5 Ti-6Al-4V (15-53 μm) powder with the printing parameters in Table 3. The samples were identified as followed QTA01.03 and QTA01.08 were produced in build one which

contained nine total artifacts (Figure 11) while build 2, 3, and 4 only had one artifact in the build and represent QTA03.01, QTA04.01, and QTA05.01 built in the center of the build plate.

Table 3 Printing parameters for repeatability and reproducibility analysis

Part ID	**Units**	**QTA01.03**	**QTA01.08**	**QTA03.01**	**QTA04.01**	**QTA05.01**
Machine	-	SI3758 - EOS M 290				
Material		Ti6Al4V				
Build time	[hr]	22	22	6.5	6.5	6.5
Deposition Velocity	[mm/s]	150				
Layer Thickness	[mm]	0.03				
Plate Location X	[mm]	**210**	**125**	125		
Plate Location Y	[mm]	**40**	**210**	125		
Global Offset	[mm]	0.1				
Hatch Offset	[mm]	0.015				
Rotation Angle	°(degrees)	67				
Inner Contour Power	[W]	150				
Inner Contour Offset	[mm]	0.02				
Inner Contour Speed	[mm/s]	1250				
Outer Contour Power	[W]	150				

Outer Contour Offset	[mm]	0.0
Outer Contour Speed	[mm/s]	1250
Scan Order	-	infill>inner contour>outer contour>, edge
Scaling Factor	-	X=1.000 Y=1.000 Z=1.000

Figure 11 Printing array QTA01.03 & QTA01.08.

The mathematical representation of each geometric characteristic according to GD&T ASME Y14.5 was used for measurement. Vertical and horizontal distances from the datum to the

center of cylinders “A” and “B” for the true position were defined as observed in Figure 12. Cylindrical tolerance was measured with two concentric circles defined with 9 degrees lines from the base.

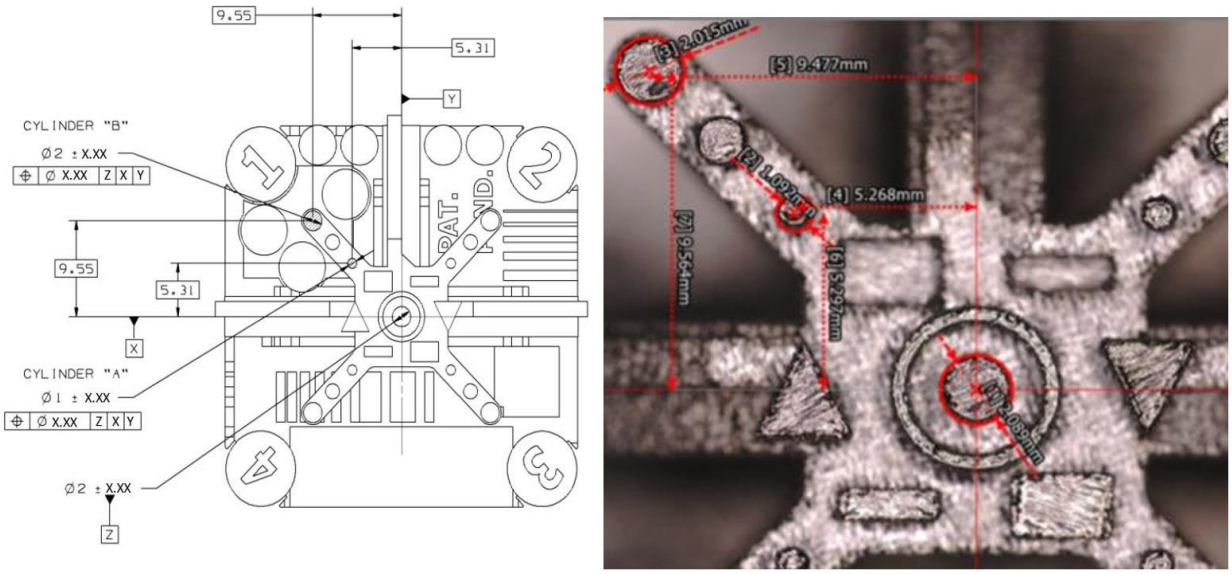

Figure 12 Top view dimensioning and tolerancing according to ASME Y14.5 for cylindrical features “A” and “B”

Comparison of contact and non-contact measurement systems

This section compared the measurement values of CMM, XCT, Optical, and Caliper methods under different surface roughness, types of features, and GD&T geometric characteristics. The measurement uncertainty was calculated based on the guide to express uncertainty in measurement (GUM) to determine the measurement variation and the limits to report dimensional sizes. The results contributed to the research questions formulated in previous sections, *What*

measurement technique is ideal for LPBF parts? and *What accuracy and precision constraints must be considered to validate the geometrical tolerances and LPBF process capabilities?*

Two qualification test artifacts from version two with different surface textures were used. The first test artifact was evaluated under as-built surface texture and the second with a surface-finished procedure as observed in Figure 13. An Optical surface roughness measurement Sa (absolute value of the difference in height of each point compared to the arithmetical mean of the surface area) was included as a reference to highlight differences in surface roughness between as-built and surface-finished artifacts used for this study. The surface roughness measurement was performed on Keyence VR-5200 (Keyence Corporation, Osaka, Japan), a non-contact measurement device that works based on fringe projection with the following sampling parameters, display resolution of 0.1 μm, Gaussian filter, cutoff wavelength S filter of 0.20 μm and L filter of 2.5 mm on areas of 2 mm X 2 mm. The surface-finished artifact was subjected to abrasive slurry machining, using the DeciDuo post-processing system (Buffalo, New York), to improve the surface roughness with an average of Sa=0.004 mm based on one measurement per face side (top and side faces view), while "As-built conditions with a Sa=0.011 mm based on the same measurement approach.

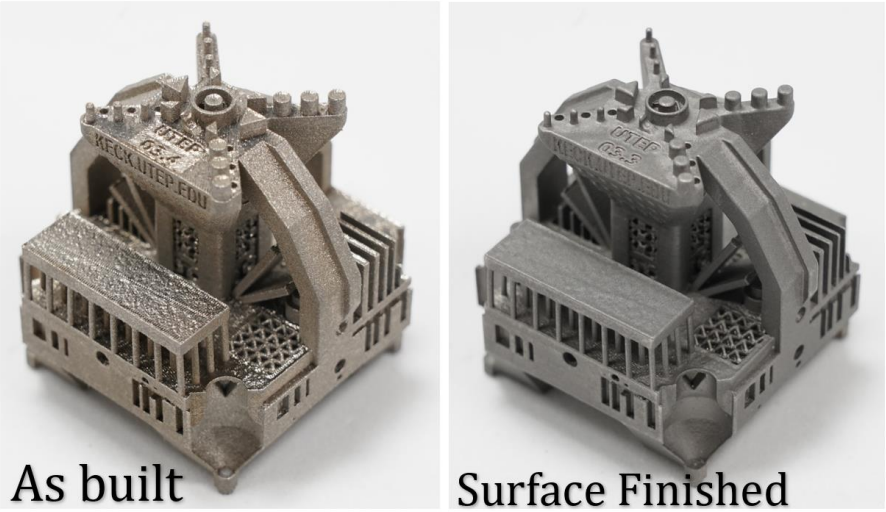

Figure 13 As-built surface roughness and surface-finished by abrasive slurry machining.

All builds were performed on an SLM 125HL (SLM Solutions GmbH, Germany) with ATI Grade 5 Ti-6Al-4V (15-53 microns) powder. The print parameters are outlined in Table 4. All offsets are measured from the ideal part boundary as defined by the .stl file.

Table 4 Printing parameters for As build and Surface finished

	Units	
Machine	-	SLM 125HL
Preheat	[°C]	200
Material		Ti6Al4V
Build time	[hr]	17.23
Layer Thickness	[mm]	0.03
Plate Location X	[mm]	0 29
Plate Location Y	[mm]	0 29
Beam Compensation (contour 1)	[mm]	0.1
Contour 2 offset	[mm]	0.18
Contour 3 offset	[mm]	0.24

Hatch Offset	[mm]	0.18
Rotation Angle	°(degrees)	67
Contour 1 & 2 Power	[W]	100
Contour 3 Power	[W]	150x
Infill Power	[W]	280
Contour 1 & 2 Speed	[mm/s]	450
Contour 3 Speed	[mm/s]	550
Infill Speed	[mm/s]	1200
Scale X		1.0021
Scale Y		1.0021
Scale Z		1.0011

Geometrical characterization

A Computer-Aided Design (CAD) model representation of the artifact was used to create a drawing according to the GD&T symbols and rules in Figures 14,15, and 16. Each dimension was assigned a unique identification "ID" 1-48 and for the true position, flatness, concentricity, cylindricity, angularity, perpendicularity, and parallelism (TRU-ID, FLA-ID, CON-ID, CYC-ID, ANG-ID, PER-ID, PAR-ID) respectively for GD&T geometry characteristics. Tolerance values were unknown and specified as X.XX on feature control frames and in size dimensions sections.

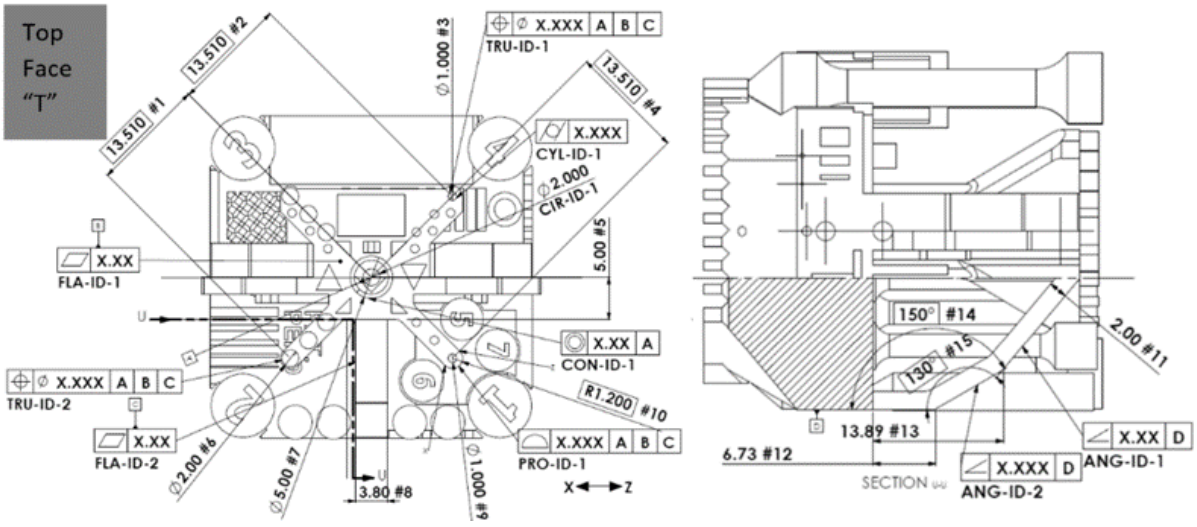

Figure 14 Top view and side angular dimensioning.

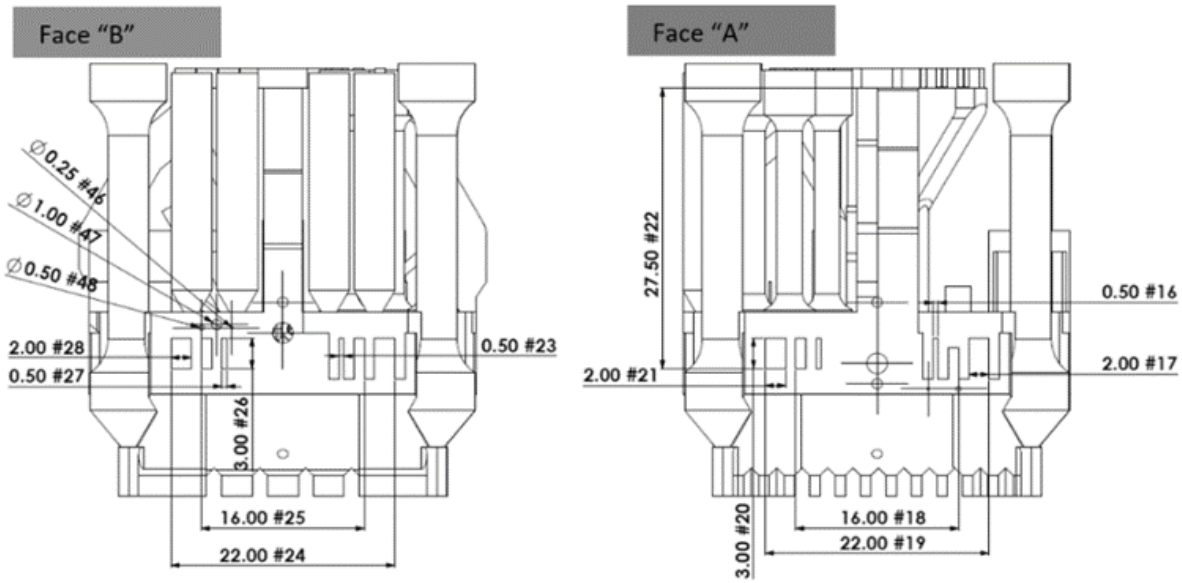

Figure 15 Face "B" and Face "A" dimensioning.

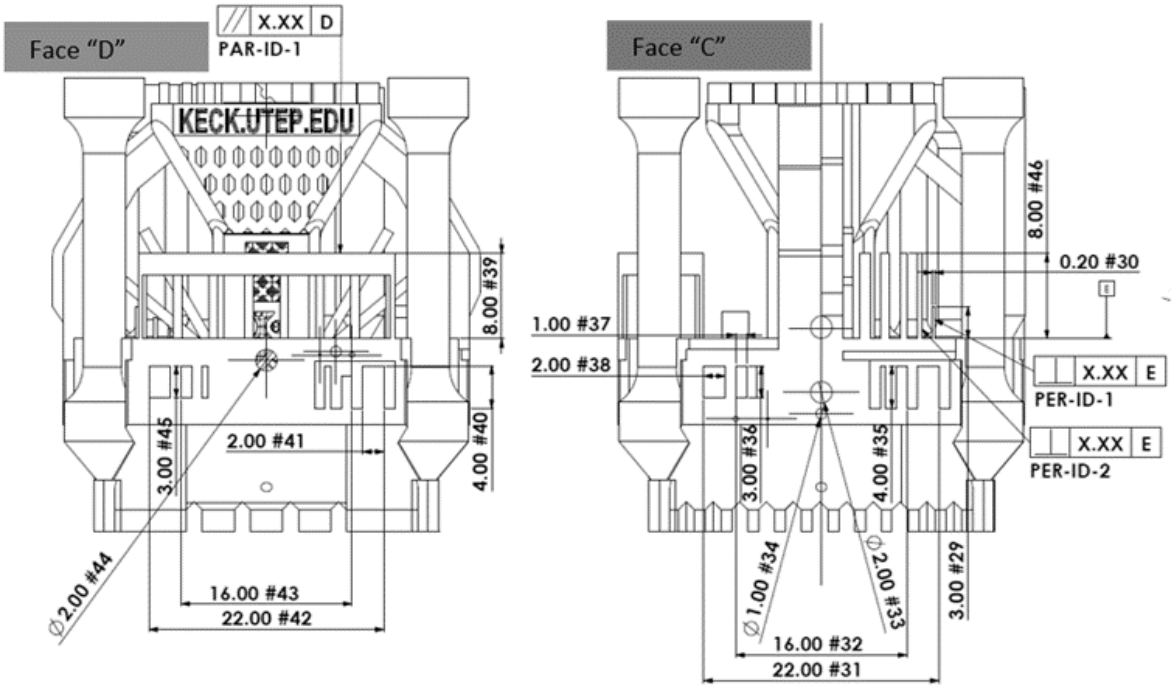

Figure 16 Face "C" and Face "D" dimensioning.

Surface texture characterization

This study evaluated different surface texture characterization approaches to determine the effect of sampling parameters (cut-off wavelength filter, evaluation length, and percentage of area evaluate). A comparison based on a qualitative analysis of the irregularities and standardized parameters was evaluated to determine the optimal sampling procedure. A novel evaluation based on cross-sectional images and mathematical processing of the surface parameters was included to compare the result with Optical surface characterization techniques. A set of functional parameters was investigated to estimate maximum and minimum irregularities distribution in combination with a contact measurement technique. This study contributes to the research question, *What factors are crucial for LPBF surface texture characterization?*

The samples evaluated are part of artifact version three from the Global Test Artifact Data Exchange Program. EOS M290 (EOS GmbH, Germany) with Scalmalloy material. Qualitative analysis was performed on the Optical measurement method previously described. Measurement in cross-sectional direction for each irregularity was performed following a Feret diameter parallel (Vertical Feret) and perpendicular (horizontal Feret) to the build plane to determine the size at the mean profile line reference as observed in Figure 17.

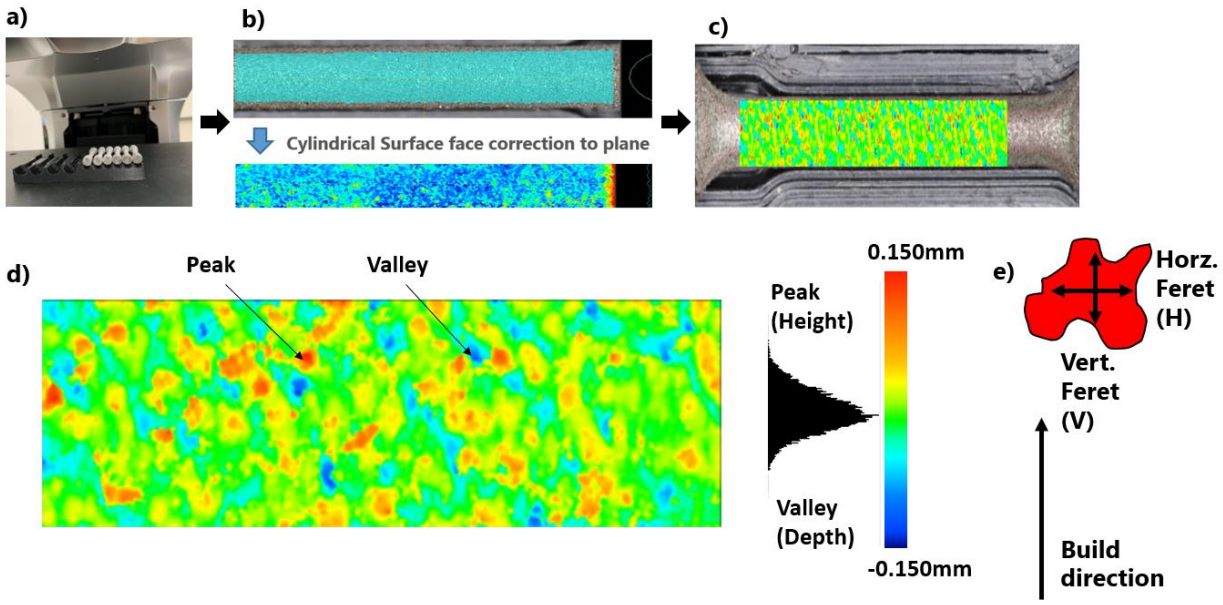

Figure 17 Qualitative Analysis: a) Keyence measuring, b) Face shape correction, c) Irregularities distribution after cylindrical to plane face correction, d) Irregularities distribution, e) Cross-sectional size characterization of irregularities.

Twenty-four different areas from six bars from two artifacts version 3 were evaluated under qualitative analysis described in the previous section. Sampling areas 1 to 12 were in the lowest center section of the printing bed and were 13 to 24 in the left center. Each bar was measured in four radial directions to cover the entire bar area as observed in Figure 18.

The tensile testing procedure was according to ASTM E8 with a diameter of 2.5+/-0.100mm and a gauge length of 10+/-0.100mm.

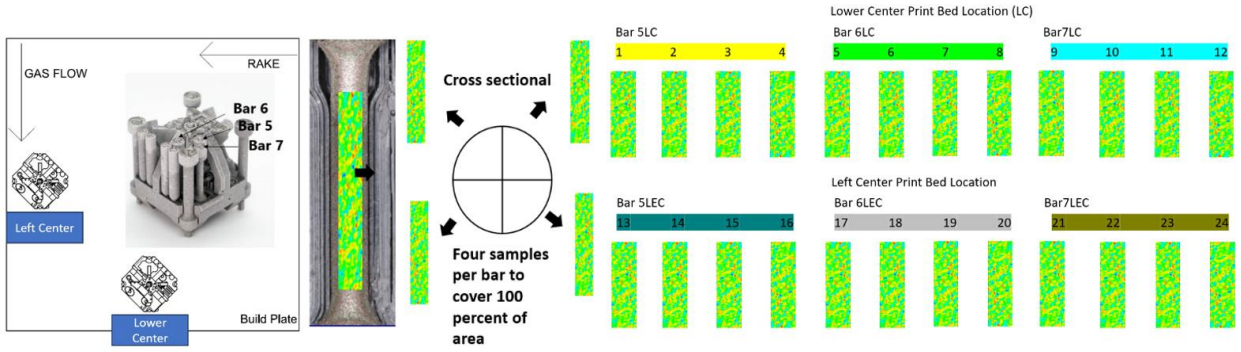

Figure 18 Samples location on the print bed and sampling section.

Optimal cut-off wavelength filter length (λc) estimation approach

Figure 19 shows the premilitary evaluation of a cross-sectional profile along an arbitrary line surface for sample ID 1. The figure shows a distribution of irregulates in varied sizes normal to the surface (Y) and in a cross-sectional direction (X). The Vertical Feret and Horizontal Feret measurement approaches were used to determine the minimum ISO cut-off wavelength (λc) filter size to cover the 95% of irregularities sizes in the X direction.

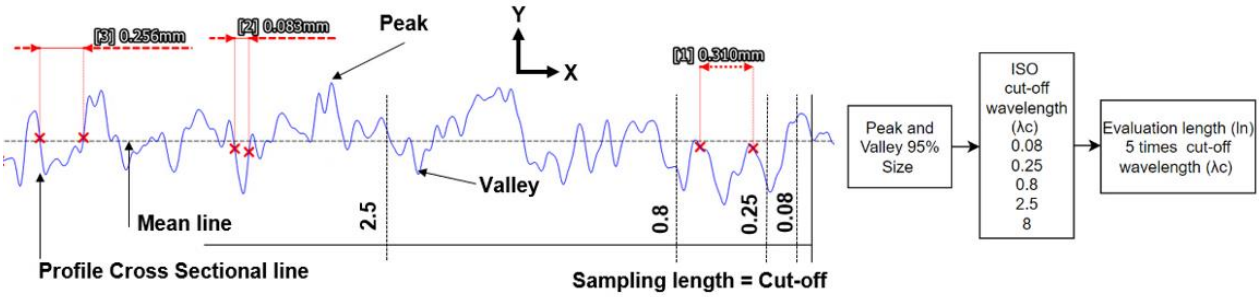

Figure 19 Cross-sectional profile obtained by the Optical method and cross-section size (X) of irregularities about the cut-off wavelength filter value.

Cross-sectional characterization

Cross-sectional images from the same batch samples were obtained to characterize the surface texture and compare the results with the bar samples. Figure 20 shows the location of the section evaluated 90 degrees from the build plate. Polished sections were prepared following the classical metallographic procedures.

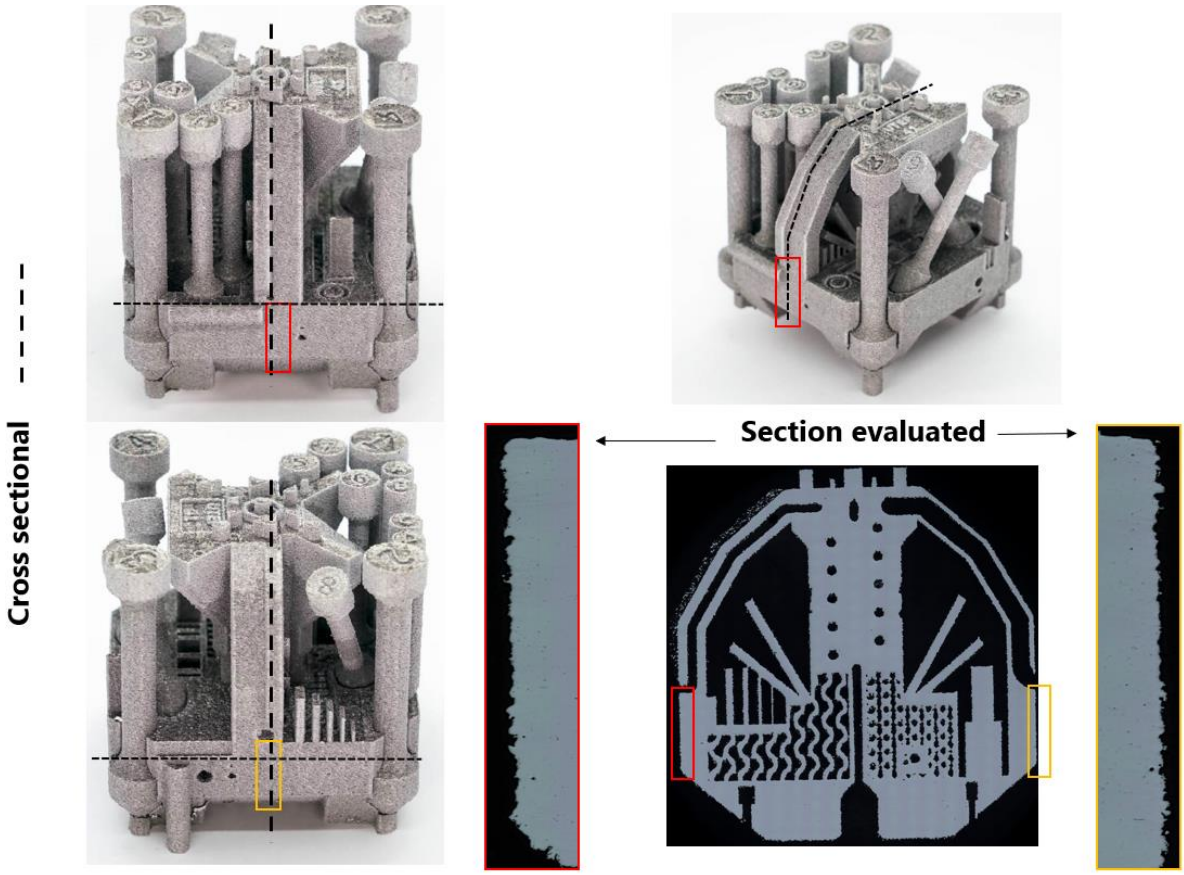

Figure 20 Cross-Sectional sampling location.

Figure 21a shows the cross-sectional images obtained by an electronic microscope with a 100X magnification, one pixel equal to 2.06 µm. Furthermore, images were imported to Image J

Software and manipulated to convert into binary and subtract the edges (Figure 21b and 21c). A manual clean was applied to eliminate pixels that are not part of the edge section to avoid noise when calculating surface parameters (Fig 21d). Scale function was applied to convert the constituent pixels into dimensional coordinates. Profile images were loaded into Python Software (see appendix for code) and processes to obtain an X-Y coordinate array.

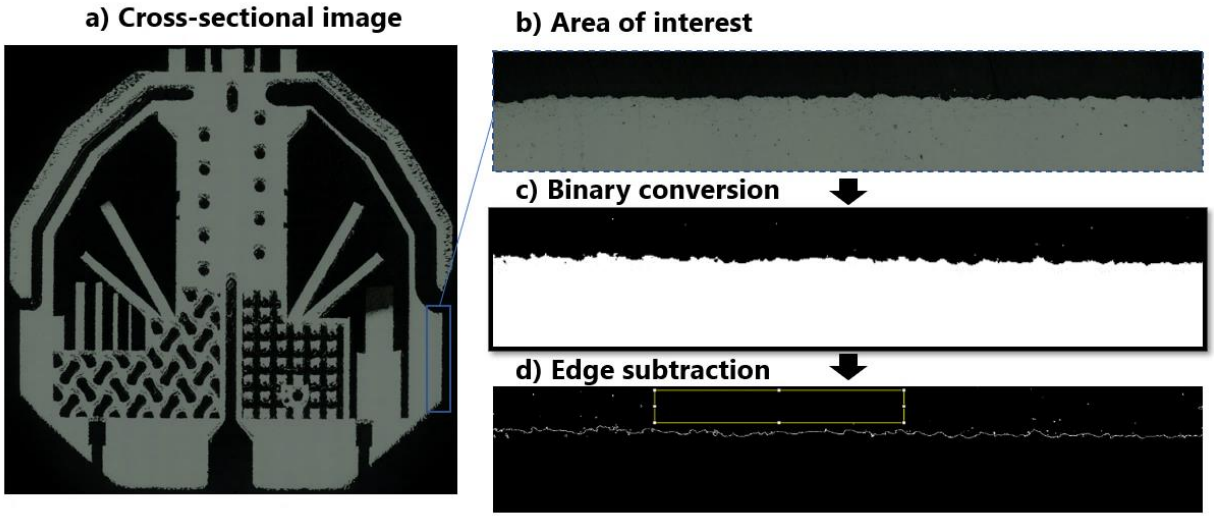

Figure 21 Profile subtraction process: a) full cross-sectional area of artifact, b) Location edge of interest, c) Binary conversation with Image J, d) edge subtraction and noise removal process.

The primary profile, which results from the subtraction of the least-squares line to the raw profile, contains both waviness and roughness components as observed in Figure 22. A Gaussian filter was used to separate the waviness from the profile and surface roughness (Eq. 9), where $\boldsymbol{\alpha}$ is a constant ($\alpha = 0.4697$) and $\boldsymbol{\lambda c}$ is the cut-off wavelength filter value, ***Ir*** *the sampling* length and ***ln*** the total evaluation length. Numerical evaluations with quantitative parameters defined by ISO 4287 were calculated with the nomenclature **(P)** profile, **(R)** roughness, and **(W)** Waviness. Arithmetic mean (Pa/Ra/Wa) Eq. (10) measures the arithmetical average of the absolute values of

the profile height deviation from the mean line on the evaluation length. Maximum profile valley deep Eq. (11) (Pv, Rv, Wv) indicates the point along the sampling length at which the profile curve is the lowest. Maximum profile peak Eq. (12) (Pp, Rp, Wp) height indicates the point along the sampling length at which the curve is highest. maximum height Eq. (13) (Pz, Rz, Wz) indicates the absolute vertical distance between the maximum peak height and the maximum valley deep along the sampling length.

Equation 9 $$\frac{1}{\alpha\lambda c}\exp\left(-\pi\left(\frac{x}{\alpha\lambda c}\right)^2\right)$$

Equation 10 $$Pa, Ra, Wa, = \frac{1}{I_r}\int_0^{Ir} |Z(x)|\, dx$$

Equation 11 $$Pv, Rv, Wv = |\min(Z(x))|$$

Equation 12 $$Pp, Rp, Wp = |\max(Z(x))|$$

Equation 13 $$Pz, Rz, Wz = Rp + Rv$$

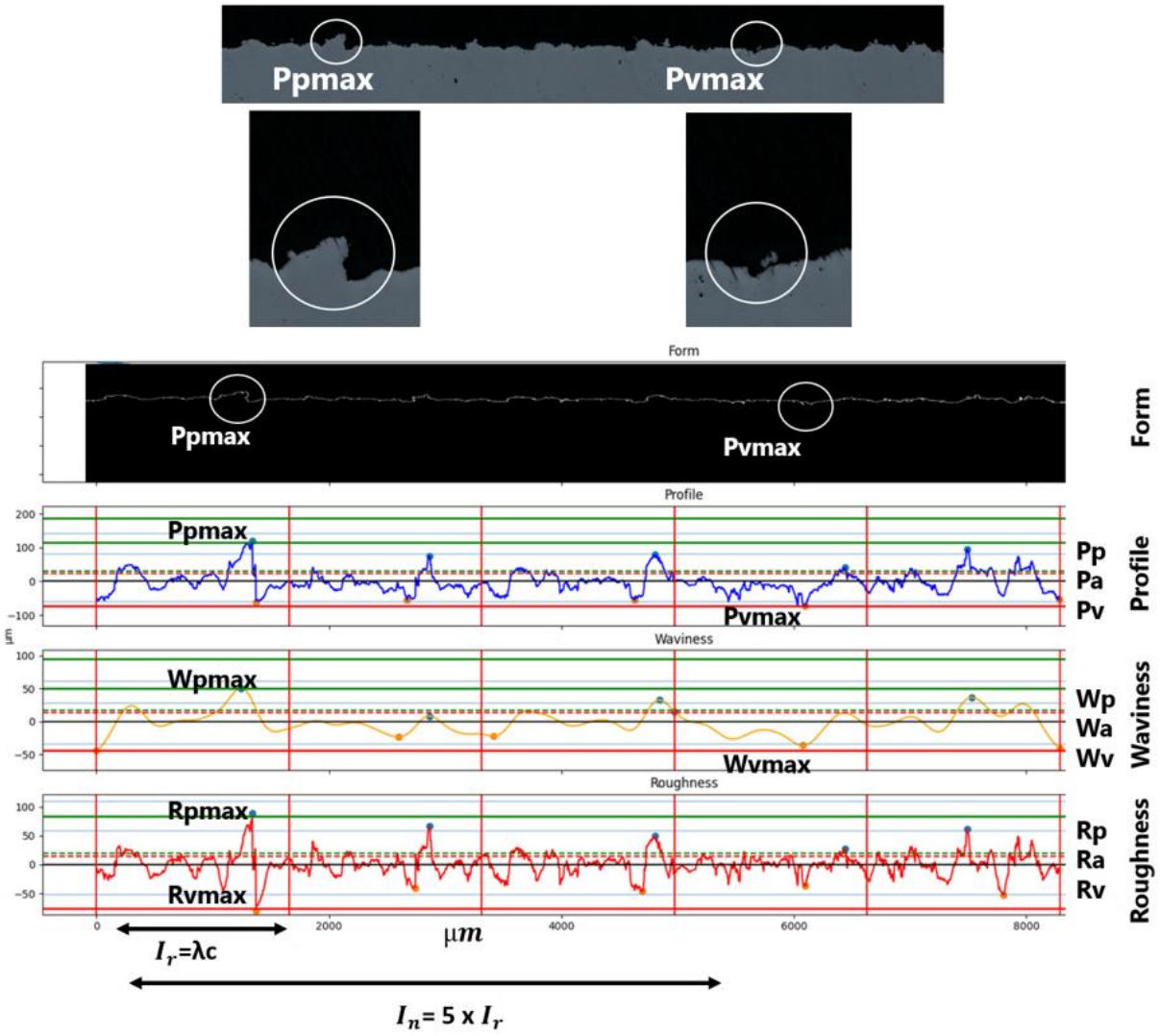

Figure 22 Cross-sectional standardized surface texture parameters calculation for profile, waviness, and roughness.

CHAPTER 4: RESULTS

Chapter 4 presents the research finds to address the research questions presented in Chapter 1. The following section contains; The results of a measuring system evaluation under a Gage R&R methodology to determine the reproducibility and repeatability of an Optical system for LPBF samples. The measurement values of CMM, XCT, Optical, and Caliper methods under different surface roughness, types of features, and GD&T geometric characteristics and the measurement uncertainty based on GUM methodology. The surface texture characterization evaluation under different sampling parameters.

REPEATABILITY AND REPRODUCIBILITY OF A MEASUREMENT SYSTEM EVALUATION RESULTS

To better understand the capabilities of the measurement system commonly used in industry applications, a Gage Repeatability and Reproducibility (Gage R&R) cross-study was performed. The results indicated that for preliminary runs the measurement system was not capable of obtaining repeatability and reproducibility for LPBF samples. The *components of variation for Gage R&R* (measurement variations related to measurement error contributors) showed values higher than 50% as observed in Figure 23. Similarly, in *Part* Operator interaction* lines were not parallel or crossed, which indicated an operator's inability to measure a part consistently and measurement error variations based on which part was measured.

The reference manual of the Optical measurement instrument specified a measurement repeatability value of 0.5 μm and a measurement accuracy of ±2 μm. However, the measurement

technique showed repeatability and reproducibility to measure the diameter of LPBF samples of 17 µm. Similarly, true position measurement with one datum reference showed an average of 28 µm of measurement error variations. These results identified the differences in measuring the system's manual accuracy and repeatability based on LPBF samples.

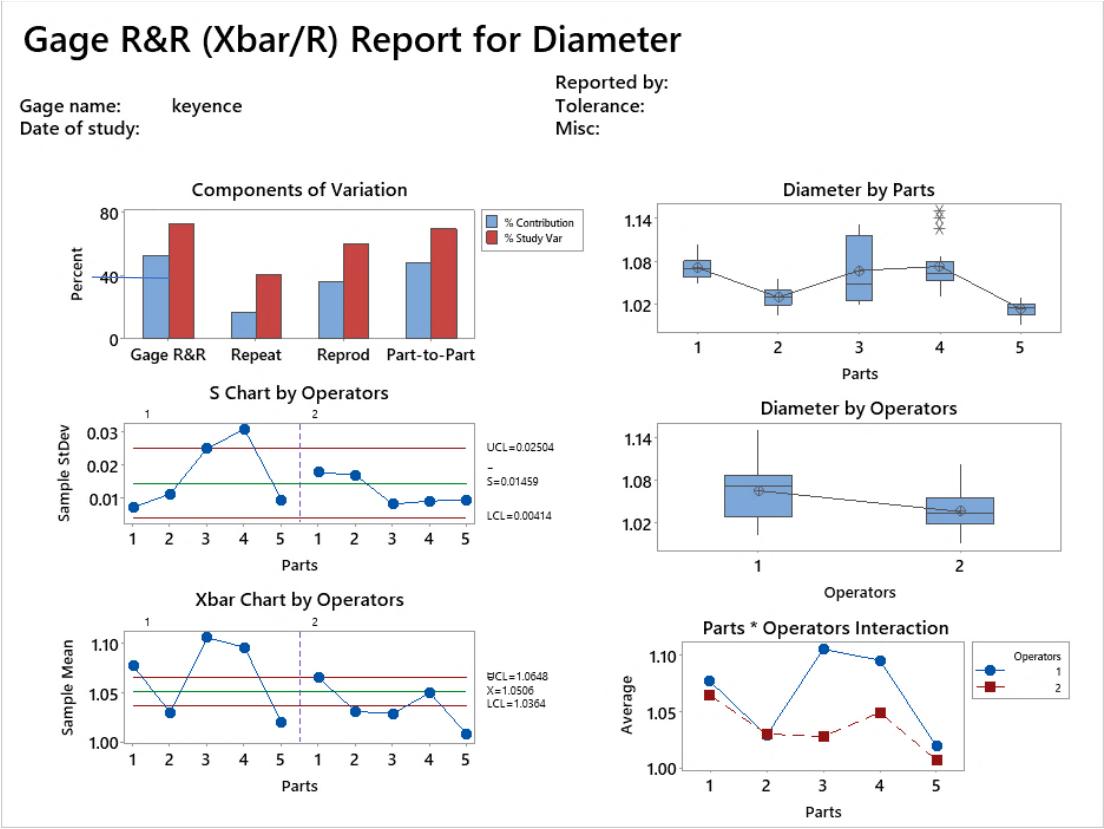

Figure 23 Gage R&R study before sampling procedure determination.

The use of Gage R&R assisted in refining the measurement process until an acceptable level of measurement error was obtained, as the results showed, following a set of sampling technique refinements, such as an edge selection definition and optimal image acquisition, a total *component of variation for gage R&R* of 5% was attained as observed in Figure 24.

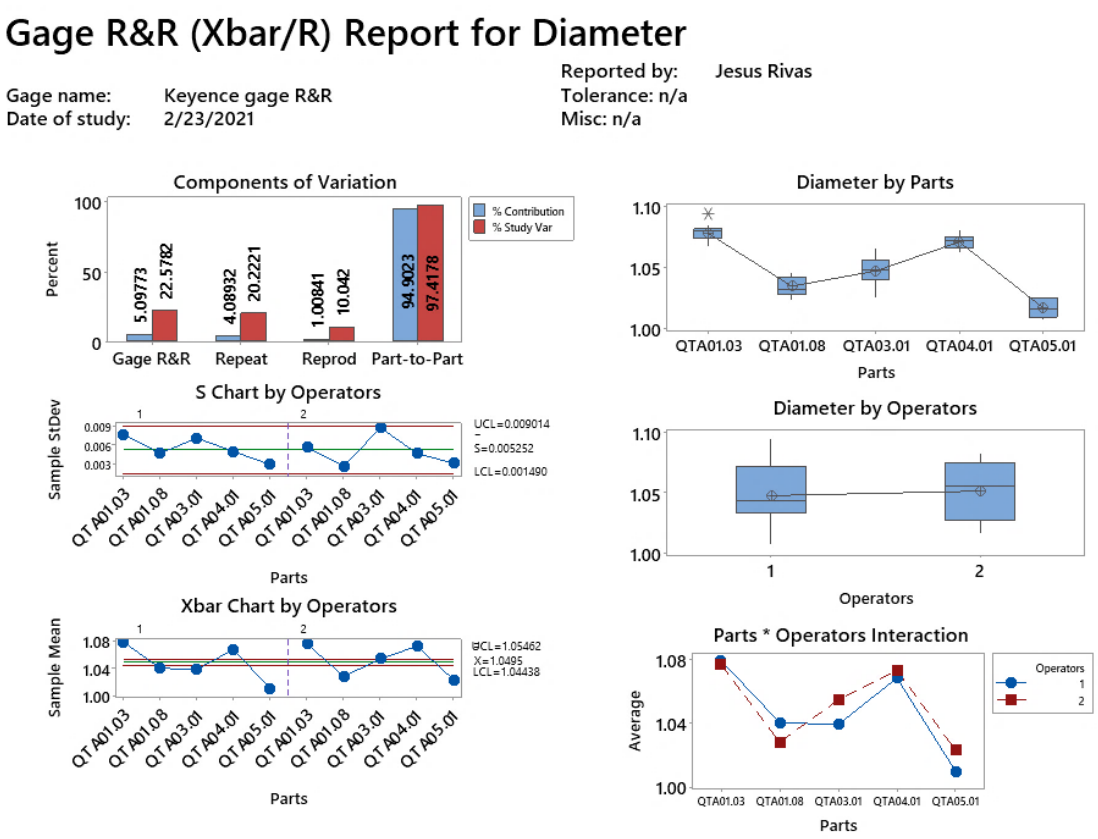

Figure 24 Gage R&R study after sampling procedure determination.

The accuracy and repeatability of the measuring method described in reference manuals based on traditional manufacturing methods cannot be transferred directly to the geometry characterization for LPBF. The confidence limit for reporting dimensional geometric values was found to be provided through the use of measuring system evaluations, and to achieve the full potential of the measuring method, sampling procedures should be enhanced based on statistical methods like gauge R&R.

COMPARISON OF CONTACT AND NON-CONTACT MEASUREMENT SYSTEMS RESULTS

The following section contains the results and considerations of the comparison of contact and non-contact measurement systems.

Coordinate Measurement Machine (CMM) as a benchmark

The comparison of different measurement methods on identical features can indicate which geometries or conditions have significant challenges to a specific measurement method. CMM was used as a benchmark against XCT, Optical Caliper, and Micrometer measurement values. According to the good practice guide, the use of a large stylus tip diameter has less measurement variation due to surface texture. However, one consideration to select the stylus tip size was to quantify the allowable deepest section to measure. As observed in Figure 25, a higher stylus tip diameter (1 mm) reported a 0.025 mm distance from the reference line, in contrast, the stylus diameter (0.2 mm) reported a distance of 0.050 mm. Based on these findings, a significant source of measurement uncertainty was found to be related to the size of the stylus tip and its ability to reach the lowest point on the surface.

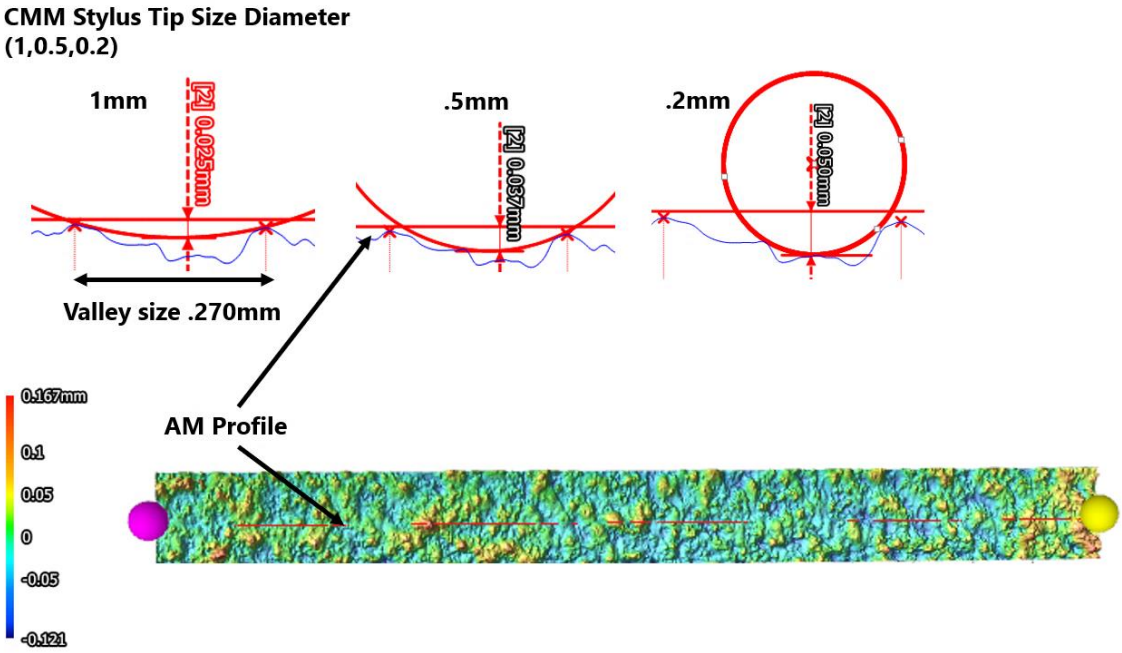

Figure 25 Effect of stylus tip size in height dimension value.

Measurement methods evaluation

Figure 26 shows the deviations from nominal (measured value minus nominal value from CAD) for the features grouped by outer diameter, outer width, height, inner diameter, inner height, inner width, and scaling factors using XCT, Optical, Caliper, and CMM where positive values indicate that feature was greater than its nominal dimension. Agreement across all four measurement methods within 25.4 µm (0.001”) was only found in outer width geometry for the as-built sample and outer diameters group for the surface-finished sample. The variability between methods was related to feature type and surface condition with overhanging type geometries (Inner height, Inner diameter) introducing the most variability. These graphs highlighted the different

reported values across the measurement methods, not only in terms of surface roughness but also in terms of the type of feature, sampling procedure, and location.

The results showed a non-particular trend variation in the measurement results between the range of methodologies with different investments in terms of capital and training. For example, less investment and training time Caliper method were in the same range as highly expensive CMM and XCT.

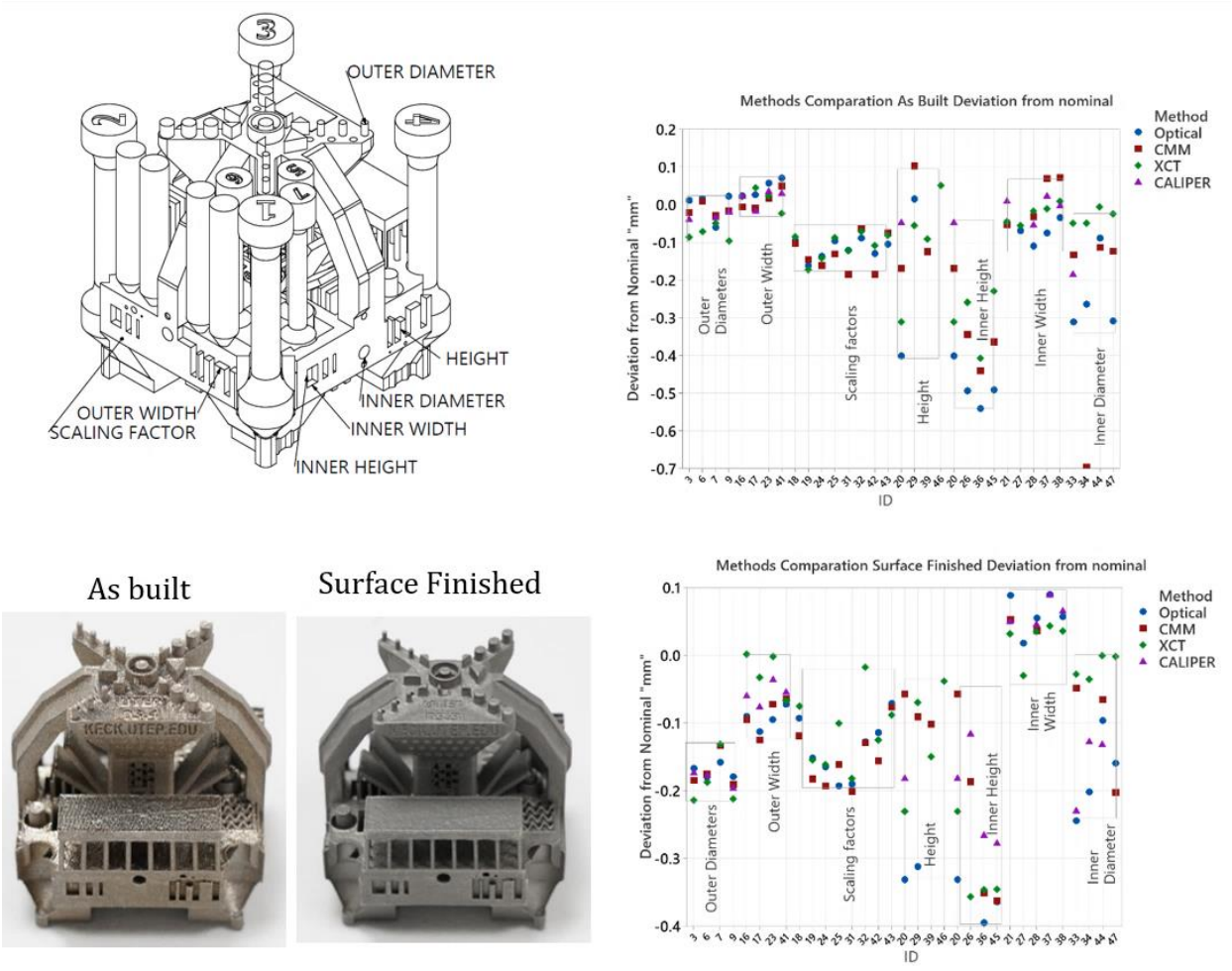

Figure 26 CMM, Optical, XC, Caliper comparison in as-built and surface-finished.

Accuracy and precision results

An accuracy calculation can estimate the variation between the measurement value from a reference value provided by a method with more precision and accuracy. Based on the difference in surface roughness between as-built and surface-finished artifacts, the XCT, Caliper, and Optical techniques produced different variations from the CMM benchmark reference value. XCT had the most variation from the CMM reference value for the as-built artifact than the surface-finished (a median value of -0.011 mm) highlighting the effect of surface roughness. The Optical method demonstrated a median deviation of 0.002 mm for the surface-finished and 0.016 mm for the as-built artifact. The Caliper method showed a median deviation of -0.013 mm for as-built compared to only 0.003 mm for surface-finished, which indicates the effect of high surface roughness on the measurement. As observed in Figure 27 for the surface finished artifact, the caliper had similar median values (similar measurement values to CMM) in comparison to expensive methods. These results highlighted the strong effect of surface roughness and the effectiveness to characterize the LPBF geometries in relation to the high investment for Optical and XCT.

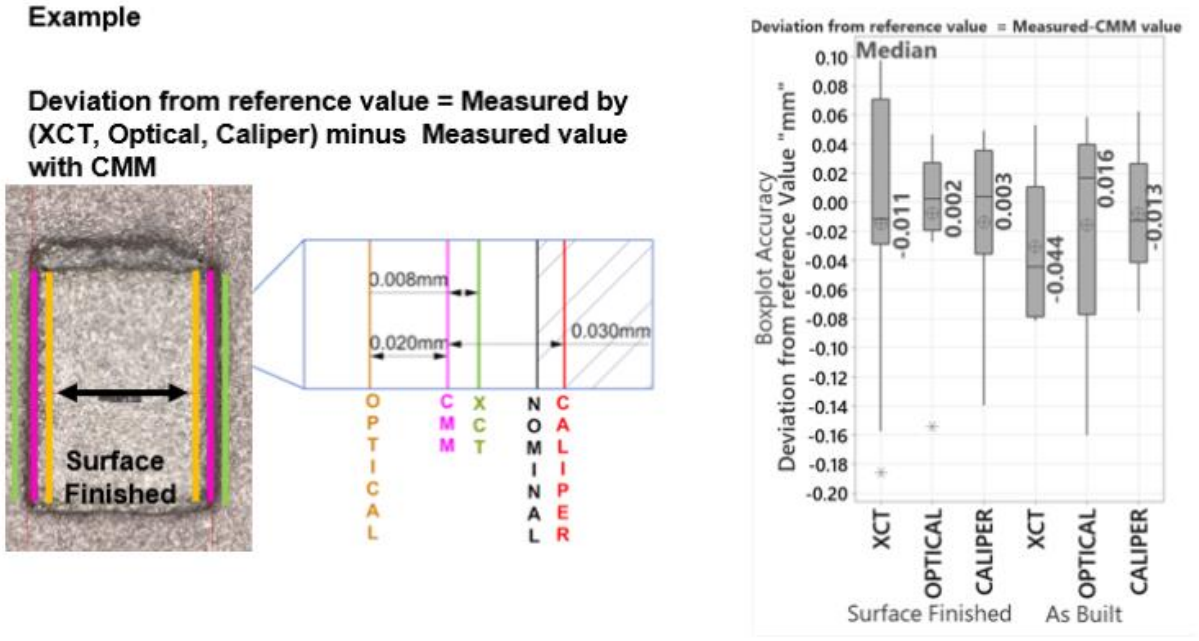

Figure 27 Deviation measurement results from CMM benchmark reference value.

Precision determination is a calculation to account for the variability of the reported measurement values. Small uncertainty values indicate high precision of the measurement system and the capacity to repeat the reported value. XCT measurements were less sensitive to the type of geometry (diameter, widths) and all measurements maintained a precision below 0.05 mm as observed in Table 5. These results indicated that XCT and Optical methods may be more precise than caliper measurements; however low uncertainty (precision) does not indicate high accuracy. The values obtained can be used as a reference based on the type of geometry and the surface condition for LPBF evaluations.

Table 5 Measurement uncertainty results

Surface-finished artifact "mm"			
Feature	**XCT Uncertainty 95%**	**OPTICAL Uncertainty 95%** *Manual reference* **High magnification of 40x (high resolution), 0.5 µm for repeatability, and measurement accuracy of ±2 µm.*	**CALIPER Uncertainty 95%** *Manual reference* **Accuracy of 25 µm, repeatability of 12 µm, and a resolution of 10 µm*
Outer diameter	0.012	0.015	0.057
Inner width	0.032	0.019	0.046
Inner height	0.017	0.020	**0.333**
Outer width	0.015	0.030	0.056
Inner diameter	0.042	**0.19**	**0.5**
As-built artifact "mm"			
Feature	**XCT Uncertainty 95%**	**OPTICAL Uncertainty 95%**	**CALIPER Uncertainty 95%**
Outer Diameter	0.022	0.064	0.036
Inner width	0.037	0.064	0.049
Inner height	0.024	0.007	**0.110**
Outer width	0.024	0.029	0.064
Inner diameter	0.046	**0.16**	**0.390**

Laser Powder Bed Fusion calibration and measurement systems limits

Beam compensation is an adjustment to account for the melt pool width of the laser beam. Figure 28 shows the beam adjustment needed to print features close to nominal sizes where insufficient or excessive beam compensation leads to an offset positive or negative between the final part boundary and the nominal size.

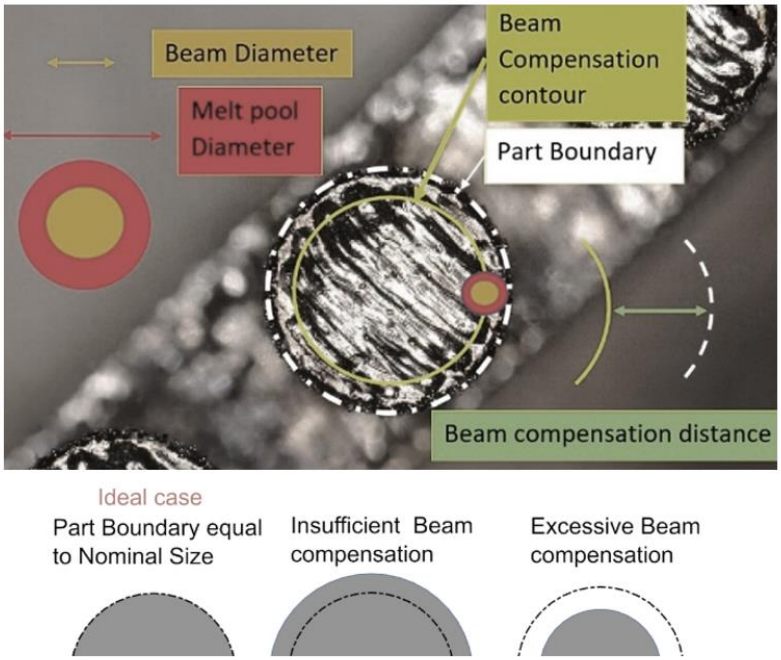

Figure 28 Beam adjustment.

Figure 29 shows the beam adjustment for a bottom section of the artifact under surface-finished and as-built conditions. The color lines represent the average beam adjustment based on the dimensions for each section and measurement methods. For surface-finished conditions, Caliper, CMM, and Optical reported a similar beam adjustment (0.090 mm) for top dimensions, where XCT showed a slightly larger value of 0.101 mm. As seen, the Optical method (0.038 mm) demonstrated the closest value to the CMM (0.044 mm), followed by Caliper (0.028 mm) and XCT (0.012 mm). CMM, XCT, and Optical reported a similar beam adjustment for bottom dimensions, where Optical showed a slightly smaller value of -0.025 mm. As observed, the differences from the highly precise and accurate method (CMM) to the least expensive method (Caliper) were below 0.020 mm for both artifacts. These results indicated that Calipers may be used to adjust beam compensation as a starting point and the use of CMM is beneficial when the tolerances capabilities of the manufacturing process and surface finishing are within 0.020 mm. Finally, the use of XCT was only recommended for applications having difficult accessing internal features while considering the deviation from the other measurement methods. The results highlighted the different beam adjustment values required depending on several factors such as the location, type of feature, surface-finished treatment, and AM process defects.

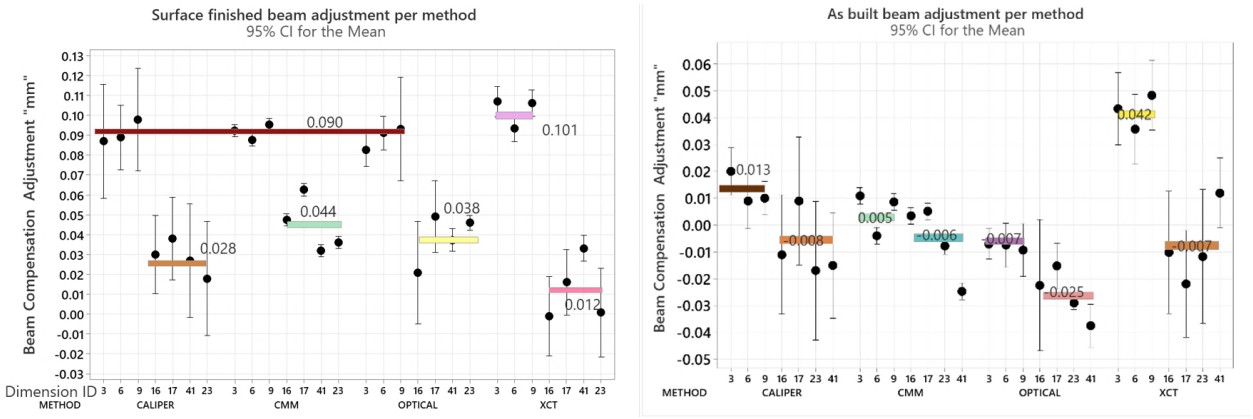

Figure 29 Surface-finished and as-built average beam adjustment estimation based on the type of measuring method.

GD&T Measurements

To compare 3D dimension measurement following GD&T characteristics, the CMM and XCT measurement methods were chosen. The investigation revealed the variations in measurement outcomes between the XCT and CMM. As seen in Figure 30, all GD&T tolerances were typically within a range of 0.050 mm when measured with CMM; however, when utilizing XCT, the tolerance range was 100% greater (0.100 mm) than CMM, which emphasized the value of sampling techniques independent of the surface texture when evaluating GD&T characteristics.

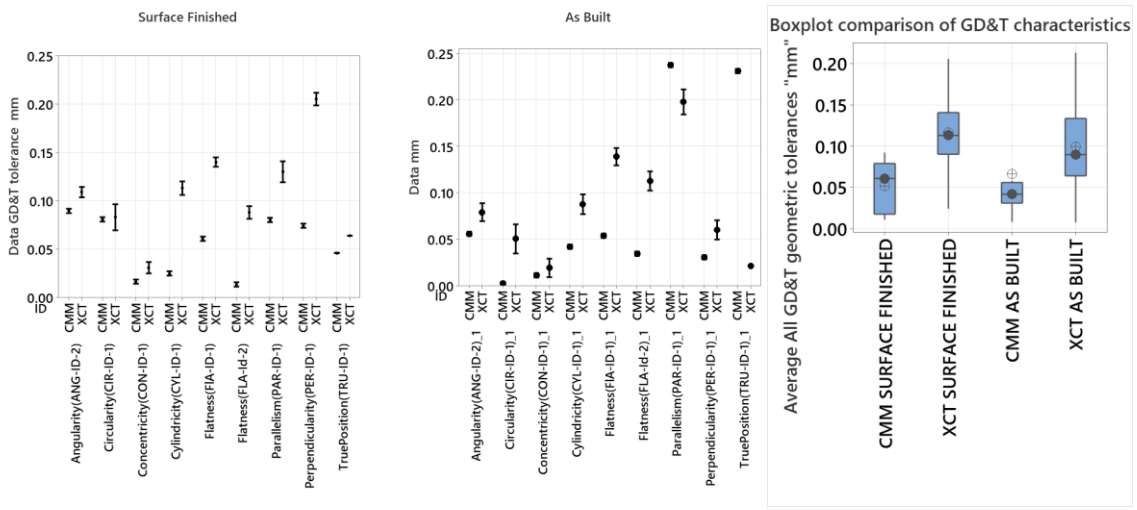

Figure 30 GD&T measurement results for the surface-finished and as-built artifacts.

SURFACE TEXTURE CHARACTERIZATION RESULTS

The following section shows the result to answer the research question, *What factors are crucial for LPBF surface texture characterization?* The section included the effect of sampling location, sampling parameters such as ISO filter predefined sizes for cut-off wavelength, or the variations between profile and areal texture characterization. Consideration to estimate the minimum and maximum size for samples used for tensile testing calculation and comparison between Optical and Cross-sectional surface roughness characterization.

Critical factors for surface texture characterization "Effect of the sampling location"

The effect of the sampling location is highlighted in Figure 31 for surface texture parameters (Ra, Rz, Rp, Rv) with the same filter and the same measuring method. Across all surface texture parameters, a variation was found due to differences in the sample line placement on the LPBF surface, for example, Ra values varied by more than 30% (Ra=14 to Ra=10). The findings emphasized the need of using many sampling locations when characterizing surface textures, sampling just one portion of the surface was not optimal for LPBF.

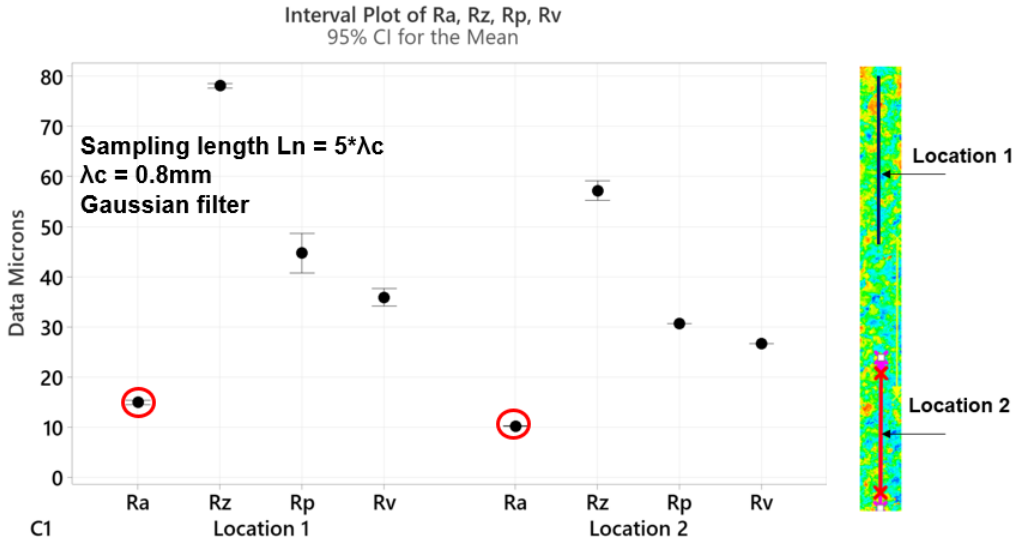

Figure 31 Sampling location effect in Ra result for the same surface.

Critical factors for surface texture characterization "Effect of sampling parameters"

Figure 32 shows the results of center position print bed samples and the bottom center position print bed samples for a profile surface texture (Ra) and areal surface texture (Sa) under the recommended ISO cut-off wavelength (λc) and sampling length *ln*.

According to the outcome, the print bed location influences the final surface roughness Ra/Sa value regardless of the filter utilized or the length of the sampling, which highlighted the necessity of characterizing samples based on the printed bed location.

A direct relationship between λc and finally Ra/Sa value was found. The smaller the filter the smaller the result value. Variation between profile (Ra) and areal (Sa) values for the same λc was observed, where the areal tends to have higher values after λc 0.25 mm size. Similarly, the differences in the area evaluated produced variations in the Sa result. The results highlighted the reproducibly effect in the values for Ra/Sa with variations regarding not only the λc size but the sampling approach and build plate location. As crucial for LPBF surface texture characterization, the filter used must be specified in the reported value, if missing this information an imprecise interpretation of the result is obtained.

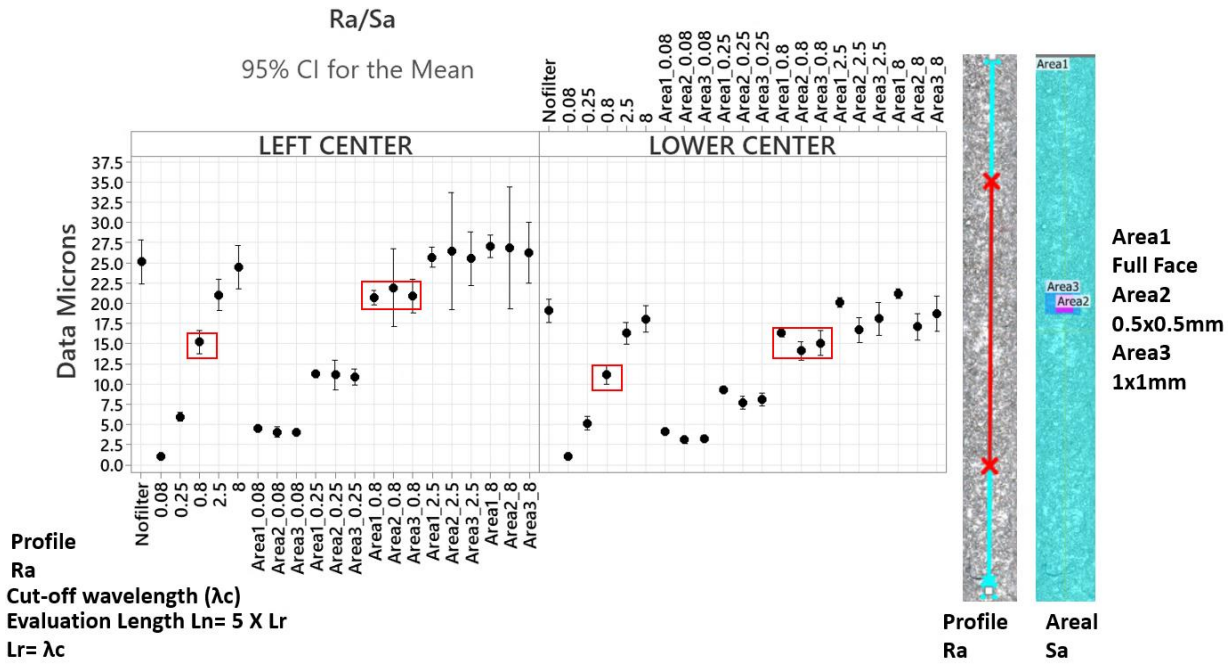

Figure 32 Surface texture variation results in Ra and Sa for the same surface.

Characterization of height and depth irregularities to determine optimal sampling parameters.

A characterization of height and depth irregularities sizes normal to the surface was performed. As observed in Figure 33 the values indicated the distribution of irregularities sizes grouped by peak height and valley depth. This distribution can be used to characterize the surface texture based on the sampling area percentage. For example, height or depth irregularities that represent less than 1% had values of more than 0.100 mm, but the average irregularities were 50% smaller. Based on the p-value (<0.005) for the probability plot the distribution does not follow a normal distribution, the skewness (0.91) and kurtosis (7.43) represent a leptokurtic distribution which indicates high core surface values and the distribution oriented in the direction of the valley. These percentage variations can be used for mechanical performance or assemblability characterization, where an isolate irregularity of 0.195 mm can be dismissed because represented less than 1% of surface irregularities. Also, this percentage highlighted from a statistical standpoint the minor probability of characterizing extreme peaks and valleys when only a proportion of the area was evaluated.

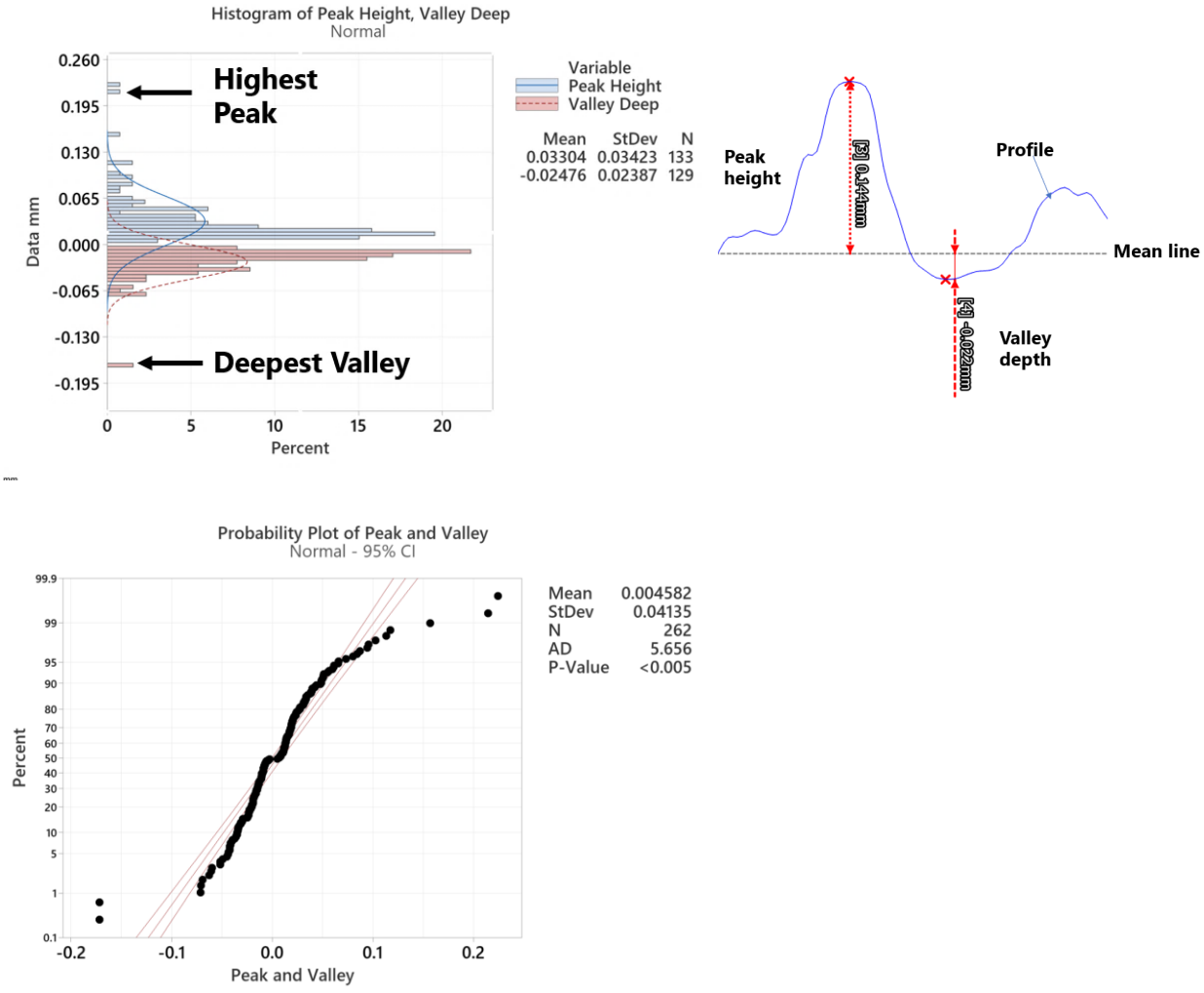

Figure 33 Irregularities in the form of peaks and valleys from the mean line.

Characterization of cross-sectional size of irregularities to determine optimal sampling parameters

Figure 34 shows the horizontal Feret and vertical Feret diameter scheme for valleys and peaks irregularities characterization in a cross-sectional direction. A higher valley size in the direction of the build plate "vertical" in comparison to "horizontal" was observed. This difference can be attributed to a layer-to-layer irregularity error in the surface and indicated a different filter needed based on the sampling direction. The results in Table 6 showed average irregularities sizes per area evaluated with values from 0.180 mm to 0.494 mm. As observed, a 0.08 mm cut-off wavelength filter value was not large enough to cover the average size of the Feret peak size, in consequence, the filter size dived in two sections irregularly, producing incorrect characterization. The results suggested the use of a cut-off wavelength filter (λc) higher than horizontal Feret and vertical Feret dimensions for correct surface characterization. As crucial factors for LPBF surface texture characterization, cross-sectional sizes can be used to obtain a reference of the optimal cut-off wavelength filter (λc). It was also observed that the cross-sectional sizes had a variation based on printing parameters such as inclination angle or printing parameters which produced the necessity of different filters size for the same sample.

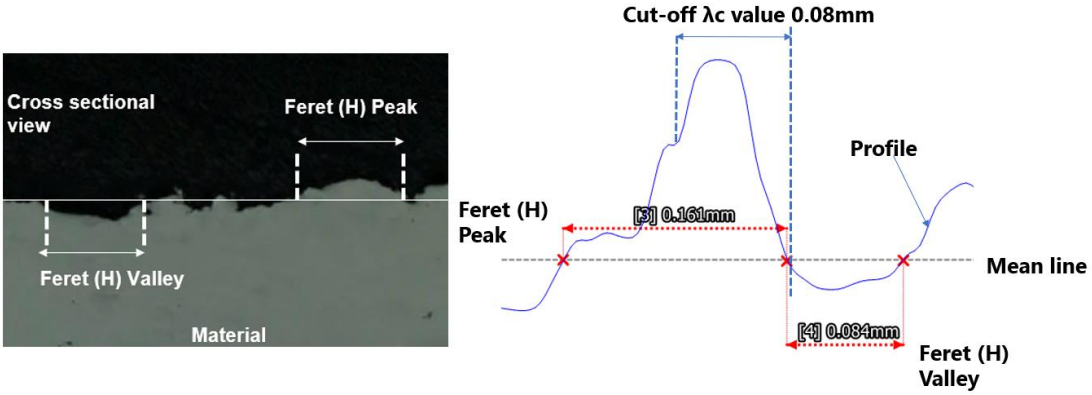

Figure 34 Cross-sectional irregularity sizes

Table 6 Feret and vertical Feret diameter result

All dimension mm									
ID	**Peak Horz. Feret**	**Peak Vert. Feret**	**Valley Horz. Feret**	**Valley Vert. Feret**	**ID**	**Peak Horz. Feret**	**Peak Vert. Feret**	**Valley Horz. Feret**	**Valley Vert. Feret**
Average	0.21	0.263	0.18	0.393	**Average**	0.226	0.254	0.183	0.494
std	0.031	0.036	0.031	0.112	**std**	0.015	0.019	0.022	0.085
Lower Center samples on the build plate					Left Center samples on the build plate				

The average irregularities depth (valleys) size with three standard deviations and the average deepest valleys were included to compare against standardized surface parameters results in Rv/Sv defined as the lowest point along the sampling profile/area in Figure 35. This surface texture parameter is relevant to correlate mechanical performance variations and crack initiation location. As the results indicated, Iso (λc) filters 0.08 mm and 0.025 mm were too small to cover

the full valley's cross-sectional size. In consequence, the use of an incorrect filter produced an incorrect characterization of the lowest point along the sampling profile.

A correct (λc) filter was proved to be in relation to the average valley horizontal and vertical Fert size (0.2 mm-0.4 mm) ~ for the samples evaluated which indicated the use of at least a filter of 0.8 mm to cover 95% of cross-sectional irregularities sizes. As observed, (λc) 0.8 mm for profile and sampling ln=5 was able to represent the average valley depth size for both sampling groups and was a better characterization of the irregularities. The result showed a direct proportion with filter size and surface percentage irregularities. The deepest valley (less than one percent of the irregularities) can be better estimated under full areal sampling evaluation Sv approach with (λc) 2.5 mm to 8 mm. The results highlighted the effect of filter sizes and full sampling area Sa versus profile line Ra.

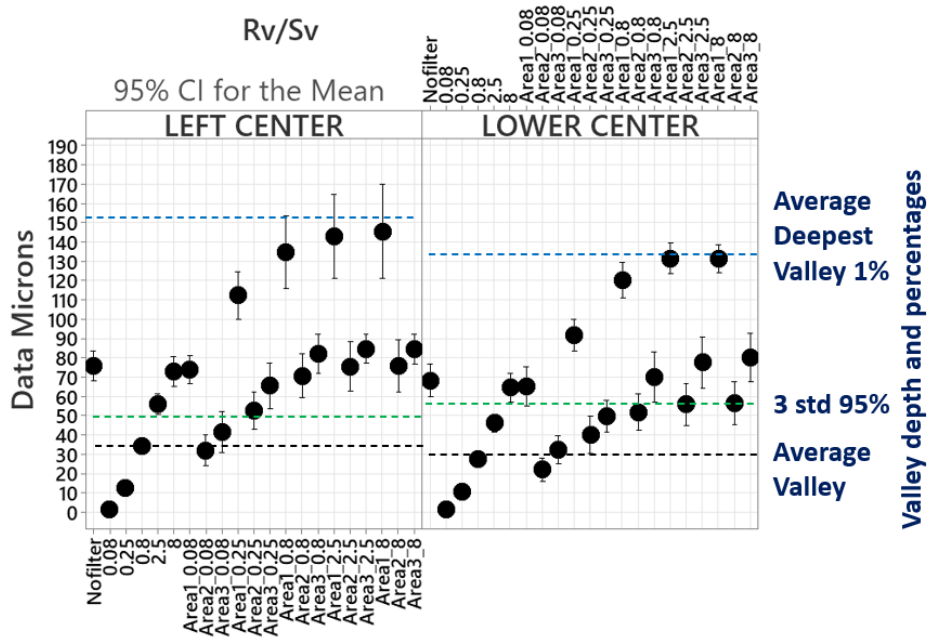

Figure 35 Surface texture parameter result variation in Rv and Sv.

Figure 36 shows the average irregularities (peaks) with three standard deviations and the average highest peaks. The values are used to compare against standardized surface parameters results in Rp/Sp defined as the highest point along the sampling. This surface parameter can be useful to form and fit assemblability estimation standpoint. Similarly, to valley characterization, Iso (λc) filters 0.08 mm, and 0.025 mm were too small for the mean peak cross-sectional size, as a result, the Rp values obtained are less than the average peak size and with a value that did not correctly represent the surface highest irregularity. As observed, a misleading interpretation of the Rp parameter can be obtained with the use of inappropriate filter sizes. In contrast, Iso (λc) filters 0.8 mm, and 2.5 mm for profile sampling characterized the irregularities close to the mean peak size value and three standard deviations. The results also highlight the effect of sampling area for Sp (full, 0.5*0.5 mm, and 1*1 mm), where only the full area evaluated for larger filters (0.8 mm,

2.8 mm, 8 mm), values reported similar values as the highest peak. The effect of increasing two times sampling area (0.5 mm*0.5 mm to 1*1 mm) can increase the Sp value up to 0.050 mm regarding the filter used. The importance of the sampling area and the filter effect in percentage irregularity distributions was highlighted.

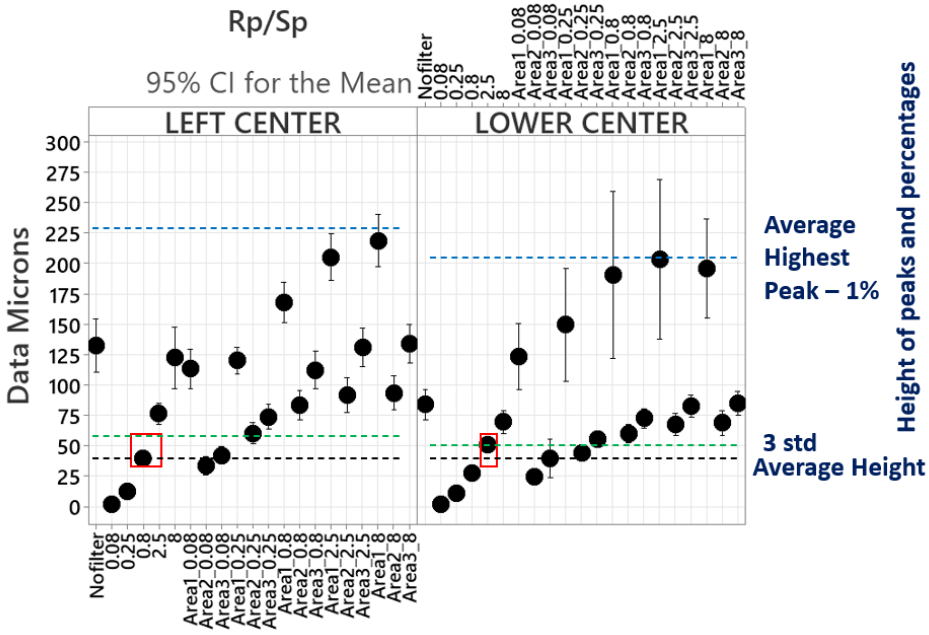

Figure 36 Surface texture result variation in Rp and Sp.

Figure 37 shows a section of the geometry where a form filter was applied, and the circular shape was converted to a line for surface roughness parameters calculations. The result showed a value of Pz=92 µm (absolute vertical distance between the maximum peak height and the maximum valley deep along the sampling length). This difference between the minimum circumscribed size and maximum inscribed size can be estimated to be two times Pz which was equal to 184 µm. This result proved the importance of defining the global size approaches

(minimum circumscribed size and maximum inscribed size) based on the application either for mechanical testing or assemblability application. As a crucial factor for LPBF surface texture characterization a global size approach must be included in the reported diameter size to reduce the measurement uncertainty.

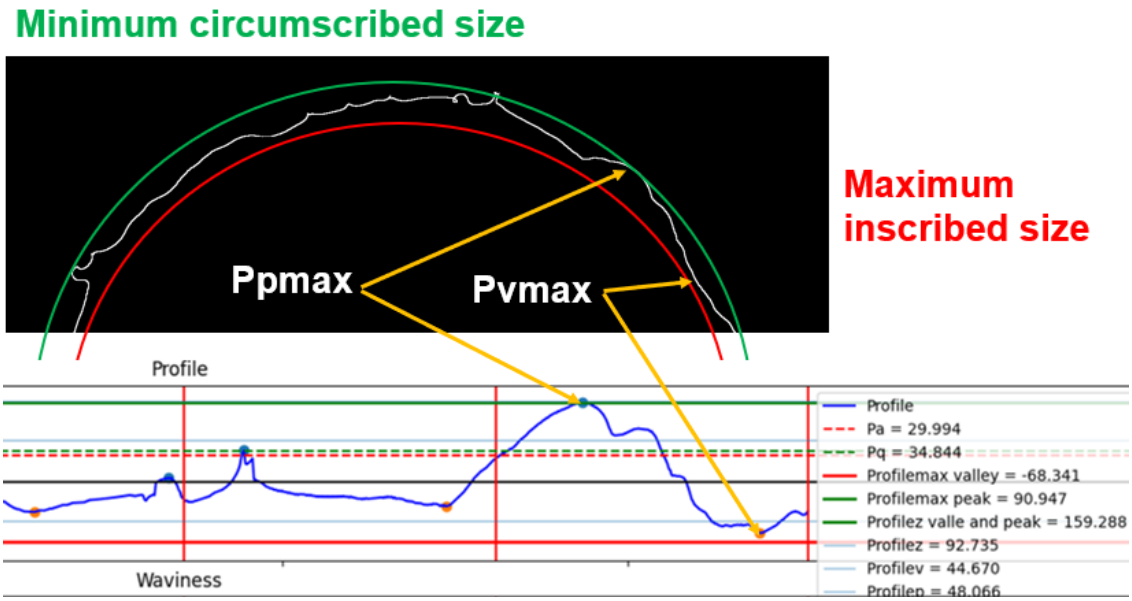

Figure 37 Difference between sizes characterization based on minimum circumscribed size and maximum inscribed size.

Considerations for size estimation

Three main contributions were identified (stylus tip size, number of samplings, and section evaluated.) as a crucial factor for dimensional size estimation. As observed in Figure 38 for a cross-sectional profile, the valley's size in combination with the stylus tip size determined a non-reachable zone, which in this case was equal to 0.026 mm.

Another contribution was the average peak and area evaluated. The Blue dashed line section defined an average height determination different than the green section based on another sampling position producing a difference of more than 0.040 mm between them. It was observed that the smaller the stylus tip size the better characterization of the profile, however, more contact points were needed to represent the surface. On the other hand, a large stylus tip size can reduce the number of sampling but increased the non-reachable zone. The results highlighted the necessity of an adjustment in the reported size to obtain a correct characterization that takes into consideration the non-reachable zone and the average peak and percentage of the sampled area.

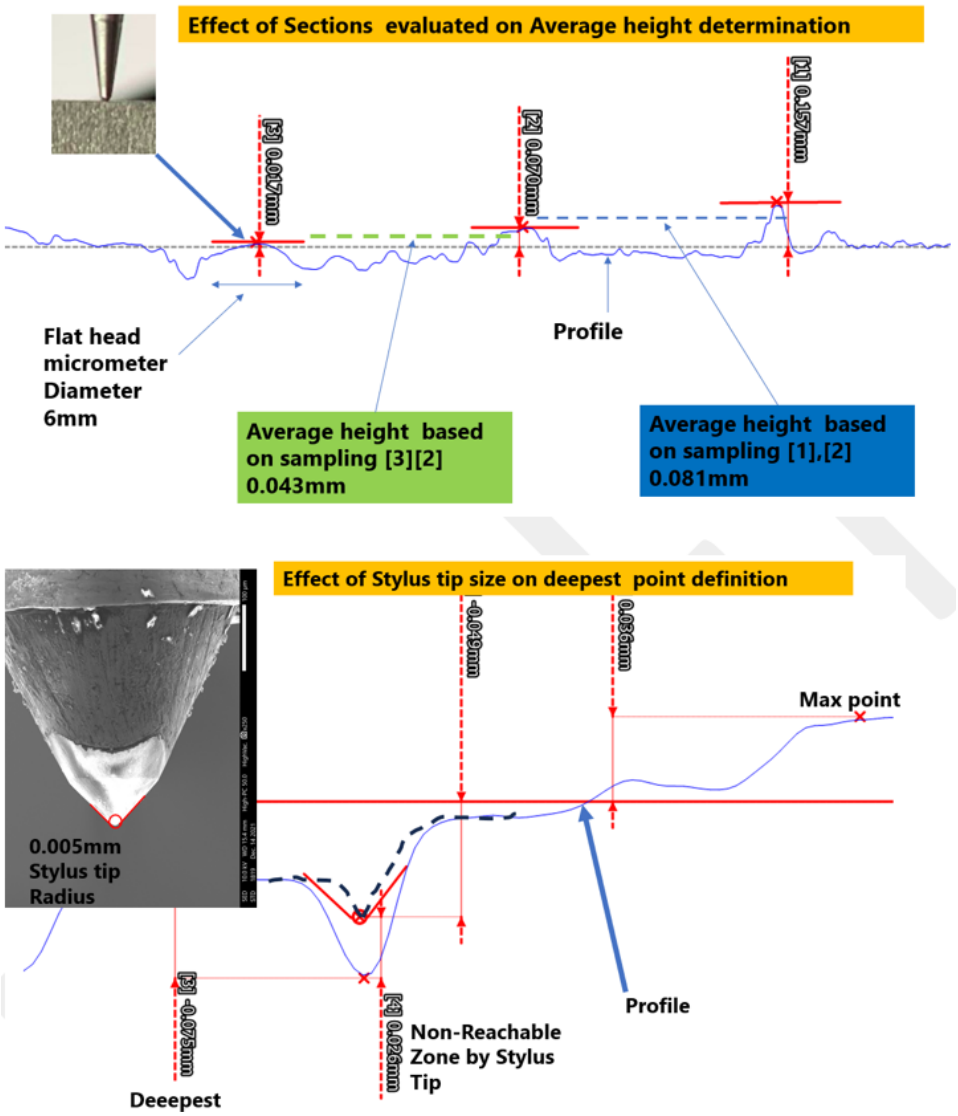

Figure 38 Effect of sections evaluated in height determination and stylus tip size in the non-reachable zone.

Figure 39 shows the average diameter size measured in a mechanical testing procedure according to ASTM E8 and the possible adjustment distance based on the non-reachable zone and the sampling percentage area described in the previous section. Since less than 5% of the area was used to measure the diameter (5 repetitions) and the contact tip size of the Micrometer was 10~ times the average cross-sectional valley size, we can estimate from a statistical standpoint that the contact point of the Micrometer was located in the average peak size, which was around 0.064 mm from the mean line of irregularities (0.00 mm). As observed in the figure, an adjusted distance can be considered to represent the non-reachable zone by the measurement device defined as (maximum inscribed size) as observed in the red line. For this example, the Micrometer reported an average diameter of 2.63 mm +/-0.017 mm (defined at the mean peak's height) and after using the adjustment distance approach a maximum inscribed diameter can only reach up to 2.44 mm diameter size, highlighting that represents less than five percent of the surface irregularities. The results showed the importance of the non-reachable zone and the sampling area evaluated in combination with the measurement method as factors to consider to accurately represent the size of a LPBF sample based on the global size approach of interest.

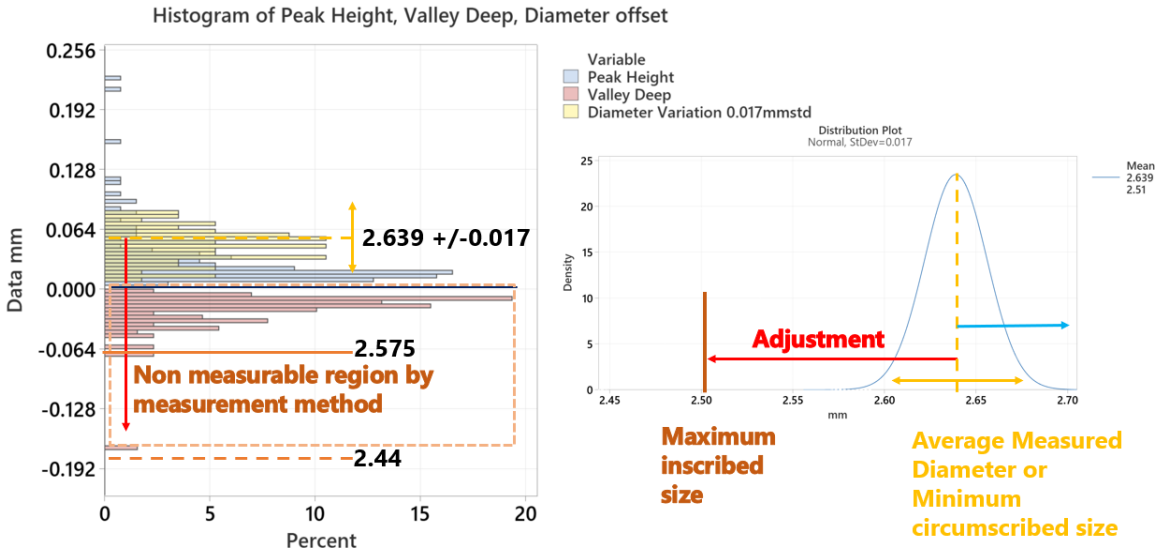

Figure 39 Diameter variations based on the average measurement and non-measurable region.

Figure 40 shows an empirical approach to determine the maximum inscribed size based on surface texture parameters and size dimension. First, Rk(.5) for profile and Sk (.5) defined as the core irregularity peak height was used in combination with Rpk/Spk to define the minimum circumscribed size defined by the measurement method based on the stylus tip size, and area evaluated. Then, the Rv/Sv parameter was combined with these parameters to estimate the deepest valley distance from the mean profile line. The final equation was (Rk(.5) + RpK + Rv) for profile and (Sk(.5) + SpK + Sv) for area. The result showed the possibilities of combining surface texture parameters and size measurements to represent different global size approaches.

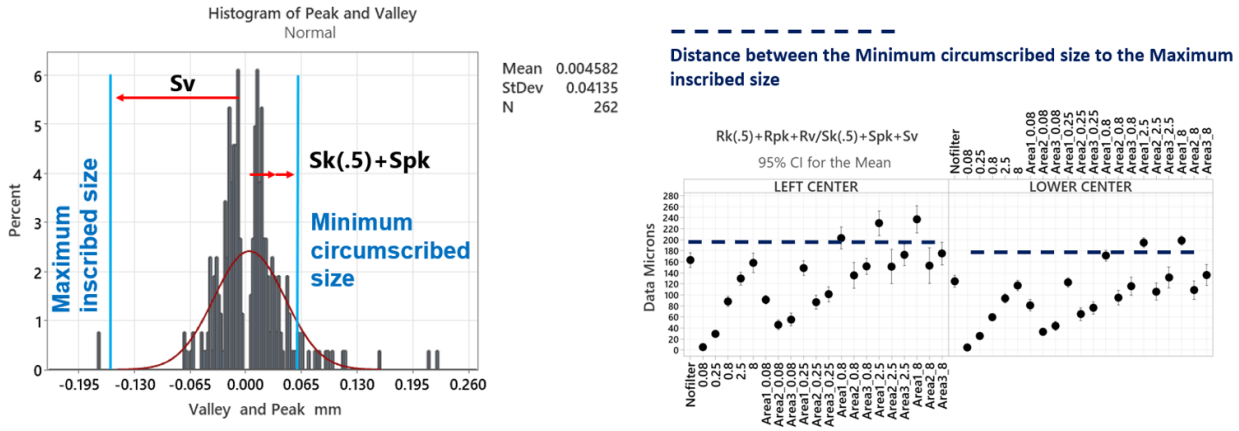

Figure 40 Empirical approach to determine the maximum inscribed size based on the surface texture parameters.

Figure 41 shows the minimum circumscribed size diameter (average diameter) measured and the maximum inscribed diameter (adjusted diameter) of the previous samples used for ASTM E8 calculation. A difference of around 0.100mm can be observed based on the different global size approaches. The stress/strain plot showed that using the average diameter can have a significant impact on the resulting stress. Overestimating the diameter of an ASTM E8 sample by 0.100 mm produced a difference in stress results of 7%. This variation highlighted the importance of correct characterization of the size dimension considering sources of measurement variations and inaccuracy such as the non-reachable zone or the percentage of sampling area as crucial factors for LPBF characterization.

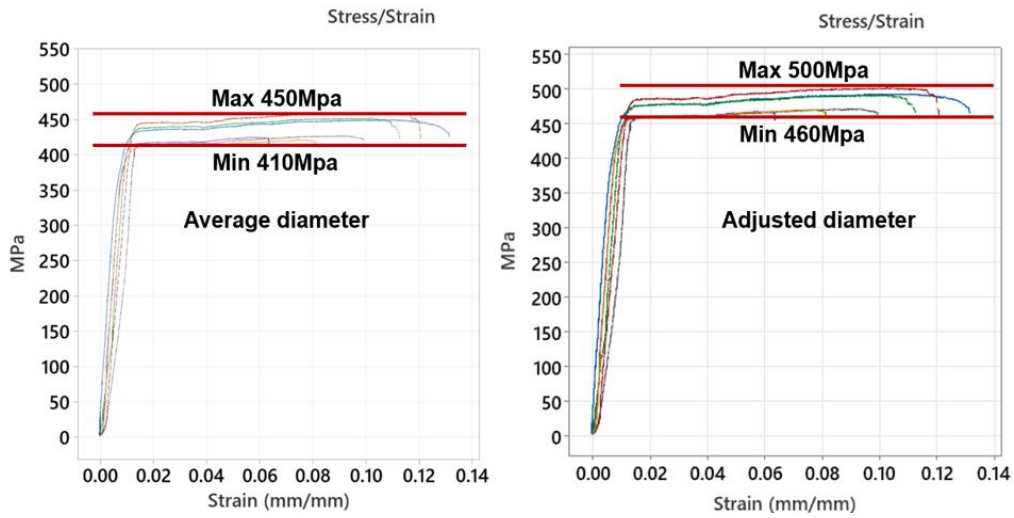

Figure 41 Effect on the tensile testing (ASTM) E8 stress results by changing the diameter size characterization.

Figure 42 shows the equivalent surface roughness parameter Ra/Sa to obtain the previous adjustment distance between the maximum inscribed size and minimum circumscribed size. As observed, filters starting at 0.8 mm showed similar values of Ra/Sa equal to 10+/-3 times and can be used to estimate that for the sample measuring method in this case a Micrometer with a stylus tip size 10~ times the average valley, an adjustment in the average reported diameters (minimum circumscribed size) equal to Ra/Sa 10 +/-3 was needed to represent a maximum inscribed diameter. The result highlights the potential use of surface texture parameters such as Ra to specify different sizes approaches.

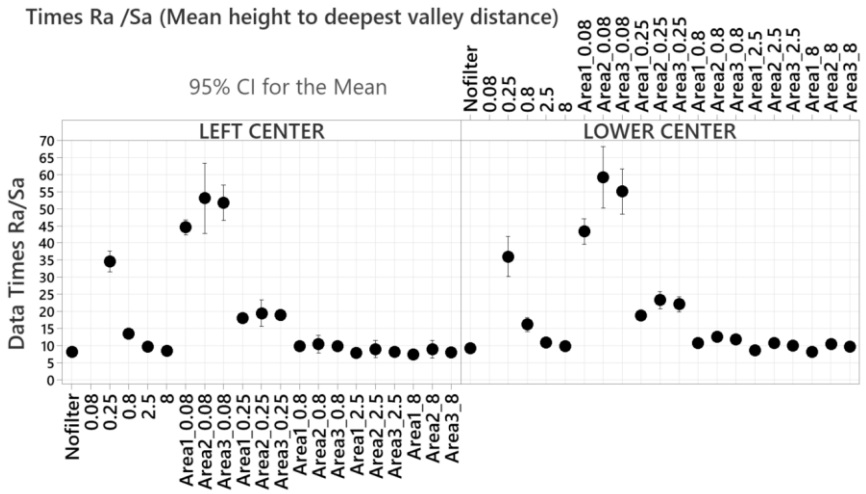

Figure 41 Equivalent surface roughness parameter Ra and Sa for maximum inscribed and minimum circumscribed size adjustments.

Novel Cross Sectional surface texture characterization results

The novel cross-sectional characterization method was able to calculate standardized surface texture parameters such as Pa/Wa/Ra/ or Pz, Wz, Rz for basic but also complex geometries with special interest for industrial applications such as lattice structures as shown in Figure 43. The novel method successfully removed from geometry to obtain a profile line and calculate the waviness and roughness based on the filter used. The novel method ensured a better geometry characterization to correlate geometrical tolerances or mechanical performance.

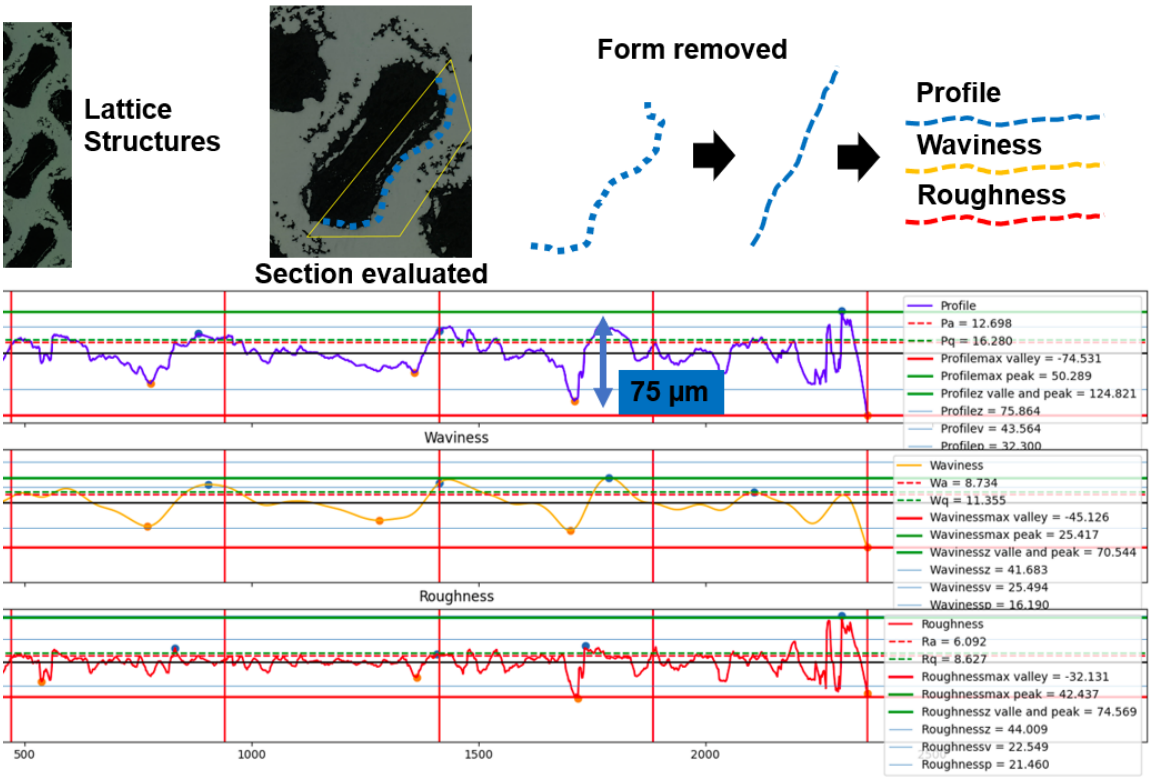

Figure 42 Cross-sectional characterization of a lattice structure section by removing the form geometry and calculating waviness and roughness.

As observed in Figure 44 a GD&T characteristic named profile can be used for irregular geometries and it is defined as two parallel surfaces separate for a tolerance value. Based on the novel characterization proposed, we can combine GD&T profile characteristics and surface texture characterization to define a tolerance range. From the previous section, the result obtained for the average Peak to average Valley (Pz) calculation across the sampling line was 0.075 mm. The surface texture (Pz) value can be used to characterize the geometry based on standardized GD&T-profile tolerance.

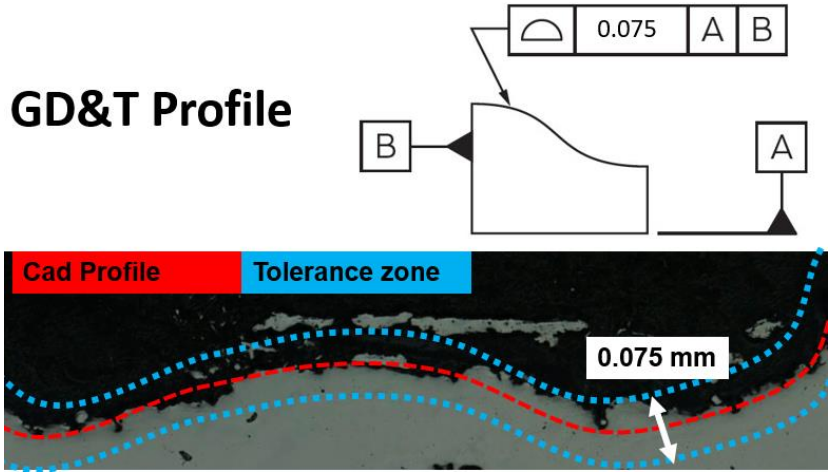

Figure 43 Profile GD&T tolerance estimation based on the novel cross-sectional characterization method.

The following sections contain the cross-sectional and Optical surface texture parameters comparison results. As observed in Figure 45, an agreement between Optical and cross-sectional with ~25 µm variation was observed for peak and valley characterization under profile, waviness, and roughness. As expected, cross-sectional characterization can reach lower irregularities than the Optical method. (It was also important to highly the impossibility to select the same cross-sectional profile line as the Optical which produced a source of error). The novel cross-sectional method proved to be able to calculate similar values to an Optical method.

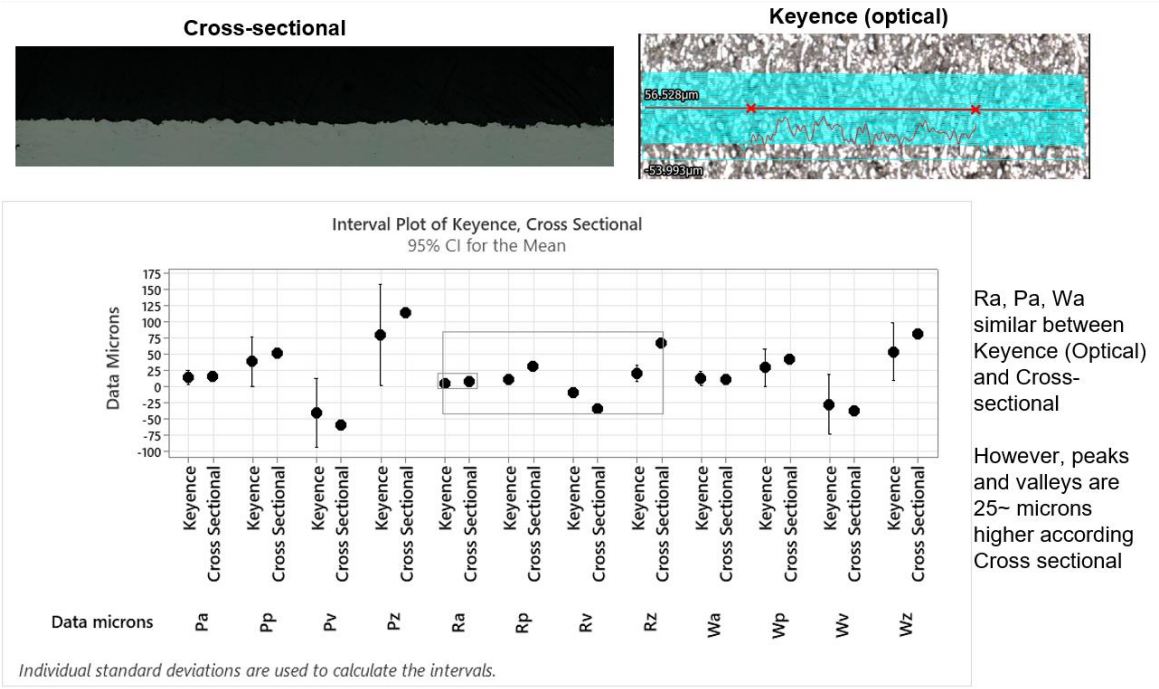

Figure 44 Surface texture parameters result in variation between novel cross-sectional and Optical methods.

Figure 46 shows the cross-sectional and reference Optical samples for Pp, for the highest peak across the evaluation length. It was observed similar values for peak characterization between

the left center and lower center build plate samples when using the cross-sectional method. However, for Optical results, there were higher Pp values for the left-center sample. The differences in these parameters results can be attributed to more attached particles on the left center that can be removed in the cross-sectional samples process. Based on the result we can conclude that the effect of the build plate location on the surface roughness was not part of the main surface edge irregularities. For mechanical evaluations, the differences in surface roughness values between print bed locations need to be evaluated to determine the effect of the sample performance. Similarly, form and fit assemblability applications need to be reviewed to determine the contribution of more attached particles on the surface based on the print bed location.

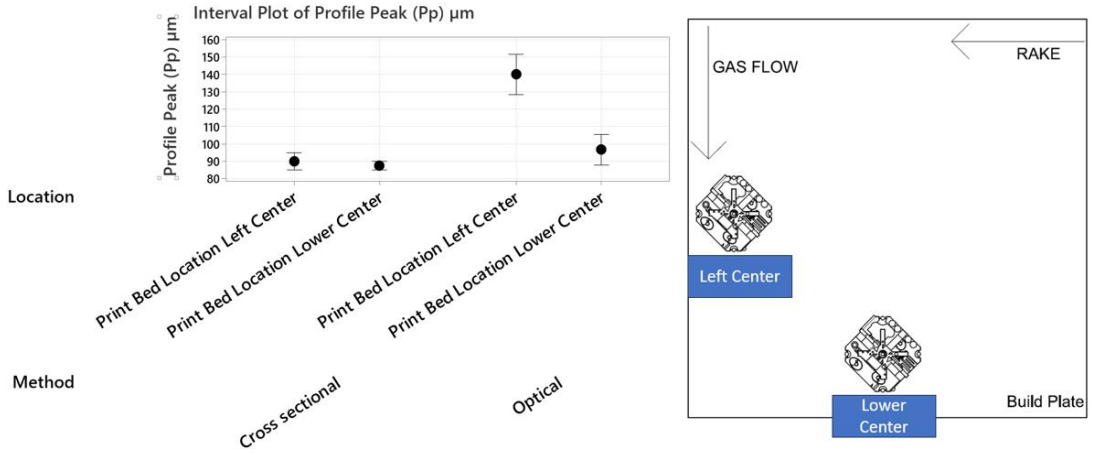

Figure 45 Effect of build plate location on peak characterization

CHAPTER 5: CONCLUSIONS AND DISCUSSION

Conclusions based on data from contact and non-contact measuring methods used to characterize the geometry and surface texture of LPBF samples are presented in Chapter 5. It has been established that additive manufacturing products with high surface roughness values affect both measurement outcomes and mechanical functionality. The surface texture characterization complexities highlighted by this dissertation helped to increase the measurement system's state-of-the-art for a precise assessment of the process capabilities required for LPBF industrialization.

Based on the findings of measuring systems evaluations, the LPBF's typical surface texture required a definition of sampling procedures and refinement for geometry characterization, and neither research nor industrial applications may directly use the manufacturer's declared repeatability and accuracy of the measurement method. To characterize the measurement system and improve the measurement process, statistical tools like the gage R&R were required.

The results showed a non-particular trend variation in the measurement results between the range of methodologies with different investments in terms of capital and training. For example, less investment and training time Caliper method were in the same range as highly expensive CMM and XCT. By utilizing statistical techniques, it was possible to reduce primary causes of error in the measurement systems, as the findings demonstrated in the improved repeatability and reproducibility values for an Optical Method. The first factor in choosing a measuring method is the tolerance range of interest for both research and industry applications. As observed in the decision tree diagram (Figure 47) fast and expensive methods can report measurement uncertainty in a range of 0.100 mm. This measurement uncertainty value is a combination of the measurement procedure, method capabilities, and a small amount of sampling area.

Following GD&T, the Optical and XCT measuring method can offer a medium uncertainty range of 0.030mm. CMM values with an uncertainty range of 0.010 mm used as benchmark reference or for direct part evaluation can be limited if the sampling produced is not defined with main considerations such as number of sample points (area evaluated), global size approach (maximum inscribed size, minimum circumscribed size) and stylus tip size.

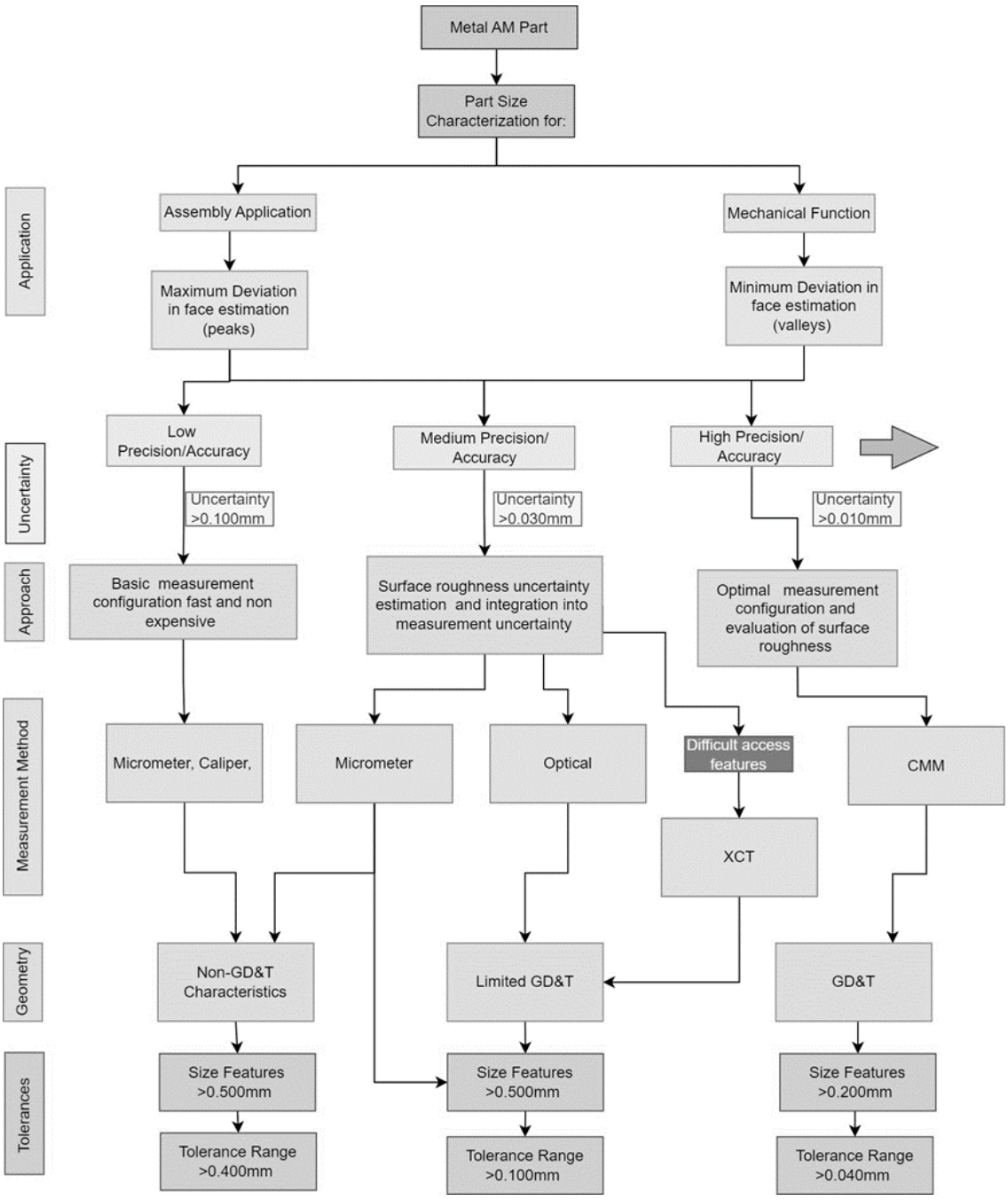

Figure 46 Measurement diagram flow based on accuracy and precision.

A combination of surface roughness measurements and size dimension measurements was proposed to represent the geometry of a surface more precisely. The results showed that the surface

of LPBF typically shows a distribution of irregularities with positive skewness and kurtosis values. This curve characterization can be used to estimate the percentages of geometrical deviations.

Cross-sectional sizes can be used to get a reference of the ideal cut-off wavelength filter, which was critical for LPBF surface texture analysis. Additionally, it was found that the cross-sectional sizes varied depending on printing characteristics like inclination angle or printing parameters, in consequence, several filter sizes may be required for the same sample.

The tensile testing evaluations showed significant variation when an incorrect diametral size was obtained. An ASTM E8 sample's diameter was overestimated by 0.100 mm, which resulted in a 7% variation in the results of the stress test. This variation brought attention to how important it was to accurately characterize a size dimension while considering potential sources of measurement error, such as the non-reachable zone or the percentage of the sampling area.

The novel cross-sectional characterization method based proved to be effective to calculate standardized surface parameters that can be connived with GD&T characteristics to define tolerances capabilities. Future research directions point to the need for additional measuring techniques, characterization, and filtering methods for attached particles, partially melted particles, and asperities from those particles to assess their contribution to mechanical behavior and geometrical form and fit properties. In conclusion, due to the randomness of irregularities found in a LPBF surface, the use of sampling approaches that can cover a full area such as an Optical is recommended more than high accuracy but limited sections evaluations such as CMM.

REFERENCES

1. Yadroitsev, I., Yadroitsava, I. & Du Plessis, A. *Basics of laser powder bed fusion*. *Fundamentals of Laser Powder Bed Fusion of Metals* (Elsevier Inc., 2021). doi:10.1016/b978-0-12-824090-8.00024-x.
2. International, A. INTERNATIONAL STANDARD ISO / ASTM Additive manufacturing — General principles — Fundamentals and. **2021**, (2021).
3. Maleki, E., Bagherifard, S., Bandini, M. & Guagliano, M. Surface post-treatments for metal additive manufacturing: Progress, challenges, and opportunities. *Addit. Manuf.* **37**, 101619 (2021).
4. Blakey-Milner, B. *et al.* Metal additive manufacturing in aerospace: A review. *Mater. Des.* **209**, 110008 (2021).
5. Leary, M. Economic feasibility and cost-benefit analysis. *Fundam. Laser Powder Bed Fusion Met.* 597–620 (2021) doi:10.1016/b978-0-12-824090-8.00022-6.
6. Abd-Elaziem, W. *et al.* On the current research progress of metallic materials fabricated by laser powder bed fusion process: a review. *J. Mater. Res. Technol.* **20**, 681–707 (2022).
7. Tahan, S. A. & Lévesque, S. Exploiting the process capability of position geometric tolerance accordingGD and T ASME Y14.5M. *2009 Int. Conf. Comput. Ind. Eng. CIE 2009* 1267–1272 (2009) doi:10.1109/iccie.2009.5223885.
8. Ameta, G., Lipman, R., Moylan, S. & Witherell, P. Investigating the Role of Geometric Dimensioning and Tolerancing in Additive Manufacturing. *J. Mech. Des. Trans. ASME* **137**, (2015).
9. Leach, R. K. *et al.* Geometrical metrology for metal additive manufacturing. *CIRP Ann.*

68, 677–700 (2019).

10. Machines, C. M., Series, C. M. & Machine, C. Coordinate Measuring Machines Coordinate Measuring Machines INDEX. 1–26 (2000).
11. Shah, P., Racasan, R. & Bills, P. Comparison of different additive manufacturing methods using computed tomography. *Case Stud. Nondestruct. Test. Eval.* **6**, 69–78 (2016).
12. Praniewicz, M. *et al.* Exploring Registration of Optical, CMM and XCT for Verification of Supplemental Surfaces to Define AM Lattices: Application to Cylindrical and Spherical Surfaces. *Procedia CIRP* **92**, 181–186 (2020).
13. Obaton, A.-F. *et al.* Reference standards for XCT measurements of additively manufactured parts. *10th Conf. Ind. Comput. Tomogr.* 0–10 (2020).
14. Schild, L., Kraemer, A., Reiling, D., Wu, H. & Lanza, G. Influence of surface roughness on measurement uncertainty in Computed Tomography. 3–10 (2018).
15. Mahshid, R., Mansourvar, Z. & Hansen, H. N. Tolerance analysis in manufacturing using process capability ratio with measurement uncertainty. *Precis. Eng.* **52**, 201–210 (2018).
16. Berez, J., Praniewicz, M. & Saldana, C. Assessing laser powder bed fusion system geometric errors through artifact-based methods. *Procedia Manuf.* **53**, 395–406 (2021).
17. Quality One International. Gage Repeatability and Reproducibility. (2021).
18. Russell, R. *et al. Qualification and certification of metal additive manufactured hardware for aerospace applications*. *Additive Manufacturing for the Aerospace Industry* (Elsevier Inc., 2019). doi:10.1016/B978-0-12-814062-8.00003-0.
19. Schleich, B. & Anwer, N. Tolerancing informatics: Towards automatic tolerancing information processing in geometrical variations management. *Appl. Sci.* **11**, 1–11 (2020).
20. Considerations, Q. A Metal Powder Bed Fusion Process in Industry : (2019).

21. Zhang, L., Zhu, H., Zhang, S., Wang, G. & Zeng, X. Fabricating high dimensional accuracy LPBFed Ti6Al4V part by using bi- parameter method. *Opt. Laser Technol.* **117**, 79–86 (2019).

22. Chen, Q., Xu, J. & Zhang, S. Cylindricity and flatness optimization for mechanical parts in additive manufacturing based on tolerance adaptive slicing. *Int. J. Adv. Manuf. Technol.* **115**, 3839–3857 (2021).

23. Rebaioli, L. & Fassi, I. A review on benchmark artifacts for evaluating the geometrical performance of additive manufacturing processes. *Int. J. Adv. Manuf. Technol.* **93**, 2571–2598 (2017).

24. Garaizar, O. R., Qiao, L., Anwer, N. & Mathieu, L. Integration of Thermal Effects into Tolerancing Using Skin Model Shapes. *Procedia CIRP* **43**, 196–201 (2016).

25. Islam, M. N. & Sacks, S. An experimental investigation into the dimensional error of powder-binder three-dimensional printing. *Int. J. Adv. Manuf. Technol.* **82**, 1371–1380 (2016).

26. Li, L. & Anand, S. Hatch Pattern Optimization of Powder Bed Fusion Additive Manufacturing Process for Minimizing Flatness error. *Procedia Manuf.* **53**, 456–465 (2021).

27. Lopes, A. C., Silva, E. C., Sampaio, Á. M. & Pontes, J. Understanding Dimensional and Geometrical Tolerances of Metal , Polymer and Composite Powder-Bed Fusion Additive Manufacturing Technologies †. 1–2 (2022).

28. Zhang, L., Zhang, S., Zhu, H., Wang, G. & Zeng, X. Investigation on the angular accuracy of selective laser melting. *Int. J. Adv. Manuf. Technol.* **104**, 3147–3153 (2019).

29. Taylor, H. C., Garibay, E. A. & Wicker, R. B. Toward a common laser powder bed fusion

qualification test artifact. *Addit. Manuf.* **39**, 101803 (2021).

30. Yang, L. & Anam, M. A. An investigation of standard test part design for additive manufacturing. *25th Annu. Int. Solid Free. Fabr. Symp. &#65533; An Addit. Manuf. Conf. SFF 2014* 901–922 (2014).

31. Weaver, J. *et al.* Quantifying accuracy of metal additive processes through a standardized test artifact. in *Solid Freeform Fabrication 2017: Proceedings of the 28th Annual International Solid Freeform Fabrication Symposium - An Additive Manufacturing Conference, SFF 2017* 2273–2288 (2017).

32. Gradl, P. R. *et al.* Geometric Feature Reproducibility for Laser Powder Bed Fusion (L-PBF) Additive Manufacturing with Inconel 718. *Addit. Manuf.* **47**, 102305 (2021).

33. Kozhuthala, J. *et al.* Build position-based dimensional deviations of laser powder-bed fusion of stainless steel 316L. *Precis. Eng.* **67**, 58–68 (2021).

34. Das, P., Chandran, R., Samant, R. & Anand, S. Optimum Part Build Orientation in Additive Manufacturing for Minimizing Part Errors and Support Structures. *Procedia Manuf.* **1**, 343–354 (2015).

35. Fotovvati, B. & Asadi, E. Size effects on geometrical accuracy for additive manufacturing of Ti-6Al-4V ELI parts. *Int. J. Adv. Manuf. Technol.* **104**, 2951–2959 (2019).

36. Rupal, B. S., Ahmad, R. & Qureshi, A. J. Feature-Based Methodology for Design of Geometric Benchmark Test Artifacts for Additive Manufacturing Processes. *Procedia CIRP* **70**, 84–89 (2018).

37. Afazov, S., Denmark, W. A. D., Toralles, B. L. & Holloway, A. Distortion prediction and compensation in selective laser melting. *Addit. Manuf.* **17**, 15–22 (2017).

38. Ortega Delgado, M. A. & Lasagni, A. F. Reducing field distortion for galvanometer

scanning system using a vision system. *Opt. Lasers Eng.* **86**, 106–114 (2016).

39. Moylan, S., Slotwinski, J., Cooke, A., Jurrens, K. & Donme, M. A. Proposal for a standardized test artifact for additive. *Solid Free. Fabr. Symp.* 902–920 (2012).

40. JCGM-BIPM. Evaluation of measurement data — Guide to the expression of uncertainty in measurement. *Int. Organ. Stand. Geneva ISBN* **50**, 134 (2008).

41. ASQC Task Force, A. I. A. G. *MEASUREMENT SYSTEMS ANALYSIS*.

42. Lou, S. *et al.* An investigation of the mechanical filtering effect of tactile CMM in the measurement of additively manufactured parts. *Meas. J. Int. Meas. Confed.* **144**, 173–182 (2019).

43. ASME. *Product Definition for Additive Manufacturing (ASME Y14.46-2017)*. https://www.asme.org/codes-standards/find-codes-standards/y14-46-product-definition-additive-manufacturing/2022/drm-enabled-pdf (2017).

44. Flack, D. *Good Practice Guide No. 41 CMM Measurement Strategies Issue 2*.

45. Mitutoyo. Quick Guide to Precision Measuring Instruments. *J. Prosthet. Dent.* **11003**, 2003 (2003).

46. Kim, F. H., Pintar, A. L., Moylan, S. P. & Garboczi, E. J. The influence of X-Ray computed tomography acquisition parameters on image quality and probability of detection of additive manufacturing defects. *J. Manuf. Sci. Eng. Trans. ASME* **141**, 1–11 (2019).

47. Zanini, F., Sorgato, M., Savio, E. & Carmignato, S. Dimensional verification of metal additively manufactured lattice structures by X-ray computed tomography: Use of a newly developed calibrated artefact to achieve metrological traceability. *Addit. Manuf.* **47**, 102229 (2021).

48. Carmignato, S., Aloisi, V., Medeossi, F., Zanini, F. & Savio, E. Influence of surface roughness on computed tomography dimensional measurements. *CIRP Ann. - Manuf. Technol.* **66**, 499–502 (2017).

49. Villarraga-Gómez, H. Studies of Dimensional Metrology with X-Ray Cat Scan. *ProQuest Diss. Theses* 670 (2018).

50. Giganto, S., Martínez-Pellitero, S., Cuesta, E., Meana, V. M. & Barreiro, J. Analysis of modern optical inspection systems for parts manufactured by selective laser melting. *Sensors (Switzerland)* **20**, (2020).

51. Stavroulakis, P. I. & Leach, R. K. Invited Review Article: Review of post-process optical form metrology for industrial-grade metal additive manufactured parts. *Rev. Sci. Instrum.* **87**, (2016).

52. Gomez, C. *et al.* Optimization of surface measurement for metal additive manufacturing using coherence scanning interferometry. *Opt. Eng.* **56**, 111714 (2017).

53. Anon. *ASME Y14.5 (2009) Dimensioning and Tolerancing*. *ANSI Stand* (1973). doi:10.3139/9781569908167.017.

54. ISO 1101. *ISO 1101, 2012. Geometrical product specifications (GPS) — geometrical toler- ancing — tolerances of form, orientation, location, and run-out, International Organization for Standardization,*. (2012).

55. Morse, E. P. & Srinivasan, V. Size tolerancing revisited: A basic notion and its evolution in standards. *Proc. Inst. Mech. Eng. Part B J. Eng. Manuf.* **227**, 662–671 (2013).

56. Bhushan, B. Surface roughness analysis and measurement techniques. *Mod. Tribol. Handb. Vol. One Princ. Tribol.* 49–119 (2000) doi:10.1201/9780849377877-10.

57. Leary, M. *et al. 7 - Surface roughness*. *Fundamentals of Laser Powder Bed Fusion of*

Metals (Elsevier Inc., 2021). doi:10.1016/B978-0-12-824090-8.00023-8.

58. Nagalingam, A. P., Vohra, M. S., Kapur, P. & Yeo, S. H. Effect of cut-off, evaluation length, and measurement area in profile and areal surface texture characterization of as-built metal additive manufactured components. *Appl. Sci.* **11**, (2021).

59. Townsend, A., Senin, N., Blunt, L., Leach, R. K. & Taylor, J. S. Surface texture metrology for metal additive manufacturing: a review. *Precis. Eng.* **46**, 34–47 (2016).

60. Diaz, A. *Surface texture characterization and optimization of metal additive manufacturing-produced components for aerospace applications*. *Additive Manufacturing for the Aerospace Industry* (Elsevier Inc., 2019). doi:10.1016/B978-0-12-814062-8.00018-2.

61. Started, G. VR-5000 / VR-5200 User ' s Manual.

62. Saqib, S. & Urbanic, J. An Experimental Study to Determine Geometric and Dimensional Accuracy Impact Factors for Fused Deposition Modelled Parts. *Enabling Manuf. Compet. Econ. Sustain.* 293–298 (2012) doi:10.1007/978-3-642-23860-4_48.

APPENDIX

Python Code for novel cross-sectional evaluation

```
import matplotlib.pyplot as plt
import cv2
import numpy as np
from scipy.ndimage import gaussian_filter1d
from scipy.interpolate import interp1d
import math
from scipy import integrate



def FillArrayWithPixelCoords(array, color, pathImageFile):
    image = cv2.imread(pathImageFile, cv2.IMREAD_GRAYSCALE)
    _, thresh = cv2.threshold(image, 127, 255, cv2.THRESH_BINARY)
    array = np.argwhere(thresh == color)

    return array



def ShowImage(pathImageFile):
    image = cv2.imread(pathImageFile)
    filename = pathImageFile[pathImageFile.rfind('/') + 1:]
    cv2.namedWindow(filename, cv2.WINDOW_NORMAL)
    cv2.imshow(filename, image)



def SplitInXYArray(array):
```

```
    y, x = zip(*array)
    y = np.array(y)
    x = np.array(x)
    #translate to x=0
    x=x-np.min(x)
    y=y-y[0]+x

    return x, y * -1


def ObtainPolyOfRegression(x, y, grade):
    coEffs = np.polyfit(x, y, grade)
    poly = np.poly1d(coEffs)
    return poly


def SizeOfPoint(x):
    return 100 * (1 / len(x))


def PointYToOrigin(x, y, poly):
    # Ajustar una regresión lineal a los datos
    x_centered = x  # - x.mean()
    y_centered = y - poly(x)  # + poly(x.mean())
    return x_centered, y_centered


whitepixels = []
white = 255
```

```
pathImageFile = "images/44/44.2/DerechaZEdge.tif"

PixelsCoords = FillArrayWithPixelCoords(whitepixels, white, pathImageFile)
PixelInX, PixelInY = SplitInXYArray(PixelsCoords)

print("X: ", PixelInX, "Y: ", PixelInY)

# Poly of regression
poly = ObtainPolyOfRegression(PixelInX, PixelInY, 3)
PointXToOrigin, PointYToOrigin = PointYToOrigin(PixelInX, PixelInY, poly)



def SetEscale(x, y, unit):
    return x * unit, y * unit



unit = 2.06
PointXToOrigin, PointYToOrigin = SetEscale(PointXToOrigin, PointYToOrigin, unit)



def GetWaviness(y, alpha, lambdaCutoff):
    sigma = lambdaCutoff / (2 * np.log(1 / alpha))
    w = gaussian_filter1d(y, sigma=sigma, mode='nearest')
    return w



def GetRoughness(w, p):
    return p - w
```

```
def GetWaviness2(x, y, alpha, lambdaCutoff, profileFunction):

    y_weight = np.zeros_like(y)

    sampling_length = np.max(x)
    print("Cutoff: ", lambdaCutoff, "microns")
    print("Lenght: ", sampling_length, "microns")
    lenght_in_cutOffs = sampling_length / lambdaCutoff
    print("Lenght in cutoffs: ", lenght_in_cutOffs)
    lenght_in_cutOffs -= 1
    print("Final lenght in cutoffs: ", lenght_in_cutOffs)
    minInterval = lambdaCutoff / 2
    print("Min interval: ", "0-", minInterval)
    maxInterval = sampling_length - lambdaCutoff / 2
    print("Max interval: ", maxInterval, "-", sampling_length)

    # 0.8 = 0.0008 microns
    # Mayor cutoff, mas plano el waviness
    # Menor cutoff, mas detallado el waviness
    # En teoria

    lambdaCutoff /= 1000

    # print(x_filtered)
    for i in range(len(x)):
        # print(profileFunction(x[i]))
        # print(x_filtered[i])
        # print(profileFunction([i]))
        # print(profileFunction(x_filtered[i]))
```

```
    # w[i] = (1 / (alpha * lambdaCutoff)) * math.exp(-math.pi * ((y_nuevo[i]/ (alpha * lambdaCutoff)) ** 2))

    # w[i]= ()*(math.exp(-math.pi))

    # w[i] = math.exp(-math.pi * (y_nuevo[i] / (alpha * lambdaCutoff)) ** 2) / (alpha * lambdaCutoff)

    # y_weight[i] = math.exp(-math.pi * (profileFunction(x[i]) / (alpha * lambdaCutoff)) ** 2) / (alpha * lambdaCutoff)

    # if(x[i]>=minInterval and x[i]<maxInterval):


    #exponencial_value = math.exp(-1 * math.pi * (pow(2, profileFunction(x[i]) / (alpha * lambdaCutoff))))

    exponencial_value = np.exp(-1 * np.pi * (np.power(2, profileFunction(x[i]) / (alpha * lambdaCutoff))))


    # print(x[i])

    # exponencial_value = math.exp(-1 * math.pi * (pow(2, profileFunction(x[i])/ (alpha * lambdaCutoff))))

    # x_filtered.append(x[i])

    # print(exponencial_value)

    y_weight[i] = (1 / alpha * lambdaCutoff) * exponencial_value


    #                                                 y_weight[i]=(1/alpha*lambdaCutoff)*np.exp(-np.pi*(profileFunction(x[i])/alpha*lambdaCutoff)**2)

    # print(y_weight[i])


# print(len(x_filtered))


weight_function = interp1d(x, y_weight, kind="zero")

# print("X: ", x, "y: ", y_weight)

# f_convolve =np.convolve(profileFunction(x), weight_function(x), mode='same')

f_convolve = np.convolve(profileFunction(x), weight_function(x), mode='same')

# f_convolve = convolve(profileFunction(x), y_weight, mode='same')
```

```
    # print("F convolve values: ", f_convolve)
    f_waviness = interp1d(x, f_convolve, kind='quadratic')
    return f_waviness


# Función para calcular la línea media


alpha = 0.4697
lambdaCutoff = 25


def SortAndUniqueCoords(x, y):
    x_unique = np.unique(x)
    x_unique = x_unique -  min(x_unique)

    sorted_indices = np.argsort(x_unique)
    x_unique_sorted = x_unique[sorted_indices]
    # calcular el promedio de las coordenadas Y para cada valor único de X
    y_mean = [np.mean([y[j] for j in np.where(x == i)[0]]) for i in x_unique_sorted]

    return x_unique_sorted, y_mean


def InterpolateFunction(x, y):
    x_unique_sorted, _ = SortAndUniqueCoords(x, y)
    # calcular el promedio de las coordenadas Y para cada valor único de X
    _, y_mean = SortAndUniqueCoords(x, y)
```

```
    return interp1d(x_unique_sorted, y_mean, kind="quadratic")


x_unique, _ = SortAndUniqueCoords(PointXToOrigin, PointYToOrigin)
_, y_mean = SortAndUniqueCoords(PointXToOrigin, PointYToOrigin)

profile_function = InterpolateFunction(x_unique, y_mean)
waviness_function = GetWaviness2(x_unique, y_mean, alpha, lambdaCutoff, profile_function)

RoughnessY = PointYToOrigin
#ShowImage(pathImageFile)

import tkinter as tk
from matplotlib.backends.backend_tkagg import FigureCanvasTkAgg
from matplotlib.figure import Figure
import numpy as np
from scipy.interpolate import interp1d
from matplotlib.backends.backend_tkagg import NavigationToolbar2Tk

x = x_unique
y = y_mean


def update_plot():
    # Obtener los valores de los cuadros de texto
    try:
        lambda_cutoff = float(lambda_entry.get())
        alpha = float(alpha_entry.get())
```

```
    except ValueError:
        return
    #f_waviness = GetWaviness2(x, y, alpha, lambda_cutoff, profile_function)
    #f_gaussian = gaussian_filter1d(y, sigma=lambda_cutoff, mode='nearest')
    for ax in axs:
        ax.clear()
        ax.set_ylim(min(y), max(y))
##
    f_gaussian = gaussian_filter1d(y, sigma=lambda_cutoff, mode='nearest')
    f_roughness = GetRoughness(f_gaussian, y)

    func_gaussian = interp1d(x_unique, f_gaussian, kind='cubic')
    func_roughness = interp1d(x_unique, f_roughness, kind='cubic')
    func_profile = interp1d(x_unique, y, kind="cubic")
    # area=integrate(f_profile(x))

    print("funciones: ", func_gaussian, func_roughness, func_profile)

    data = {"Form": (PixelInX, PixelInY, "black"),
            "Profile": (x_unique, func_profile, "blue"),
            "Waviness": (x_unique, func_gaussian ,"orange"),
            "Roughness": (x_unique, func_roughness, "red")}

    ##

    sigma=lambda_cutoff
    #f_gaussian = gaussian_filter1d(y, sigma=sigma, mode='nearest')
    #f_roughness = GetRoughness(f_gaussian, y)
```

```
# data = {"Form": (PixelInX, PixelInY, "black"),
 #       "Profile": (x_unique, y, "blue"),
  #      "Waviness": (x_unique, f_gaussian, "orange"),
  #      "Roughness": (x_unique, f_roughness, "red")}

 # Iterar sobre los subplots y los datos correspondientes

 for ax, (title, (x, ydata, color)) in zip(axs, data.items()):
    if title == "Form":
        ax.scatter(PixelInX * unit, PixelInY * unit, label='Form', s=SizeOfPoint(PixelInX))
        ax.set_yticklabels([])
        axs[0].axhline(y=0, color="black")
        # axs[0].scattr(x, poly(x), label="Form")
        ax.set_title("Form")
        ax.legend(markerscale=30)
        ax.set_ylim(min(PixelInY * unit), max(PixelInY * unit))
    else:
        ax.plot(x, ydata(x), label=title, color=color)  # Plotear los datos
        ax.axhline(y=0, color="black")  # Agregar una línea horizontal en y=0

        if(alpha>max(x)):
           alpha=max(x)
        intervals= np.max(x)/alpha

        print("Intervals: ", intervals)
        intervals = math.floor(intervals)
        print("Intervals: ", intervals)

        #if(intervals<5):
```

```
distanceInterval = max(x)/intervals



print("---------------------------\n")
print("\n", title)
max_peaks = np.zeros(intervals)
max_valleys= np.zeros(intervals)
z_sum = np.zeros(intervals)

x_peaks = np.zeros(intervals)
x_valleys= np.zeros(intervals)

for i in range(intervals):

    inicio = i* distanceInterval
    fin = (i + 1) * distanceInterval
    ax.axvline(x=inicio, color='r')
    ax.axvline(x=fin, color='r')
    print(inicio, "-", fin)

    x_eval=np.linspace(inicio, fin, int(alpha))

    max_peaks[i]=np.max(ydata(x_eval))
    max_valleys[i]=np.min(ydata(x_eval))

    z_sum[i] = abs(np.max(ydata(x_eval))) + abs(np.min(ydata(x_eval)))
    x_peaks [i]= x_eval[np.argmax(ydata(x_eval))]
    x_valleys [i]= x_eval[np.argmin(ydata(x_eval))]
```

```
        ax.scatter(x_peaks, max_peaks)
        ax.scatter(x_valleys, max_valleys)
        print("Valleys : ", max_valleys)
        print("Peaks: ", max_peaks)
        print("Z sum: ", z_sum)
        print("-----------------\n")

        ax.set_title(title)  # Establecer el título del subplot
        ax.axhline(y=average_height(ydata(x)), color="red", linestyle="--",
                label=title[0] + "a = {:.3f}".format(
                    average_height(ydata(x))))  # Agregar la línea de la media aritmética
        ax.axhline(y=quadratic_average(x, ydata(x)), color="green", linestyle="--",
                label=title[0] + "q = {:.3f}".format(
                    quadratic_average(x, ydata(x))))  # Agregar la línea de la media cuadrática

        minValley, maxValley = PeakAndValleyHigher(ydata(x))
        #zOnly = abs(average_height(max_valleys))+abs(average_height(max_peaks))

        ax.axhline(y=minValley, color="red", linestyle="-",
                label=title + "max valley = {:.3f}".format(minValley), linewidth=2)

        ax.axhline(y=maxValley, color="green", linestyle="-",
                label=title + "max peak = {:.3f}".format(maxValley), linewidth=2)

        ax.axhline(y=DistanceInPeakAndValley(minValley, maxValley), color="green",
linestyle="-",
                label=title + "z valle and peak =
{:.3f}".format(DistanceInPeakAndValley(minValley, maxValley)),
                linewidth=2)
```

```
        ax.axhline(y= average_per_lenght(z_sum), linestyle="-",
                label=title + "z = {:.3f}".format(average_height(z_sum)), linewidth=0.5)

        ax.axhline(y= average_per_lenght(max_valleys),  linestyle="-",
                label=title + "v = {:.3f}".format(average_height(max_valleys)), linewidth=0.5)
        ax.axhline(y= average_per_lenght(max_peaks), linestyle="-",

                label=title + "p = {:.3f}".format(average_height(max_peaks)), linewidth=0.5)
        ax.legend()  # Agregar la leyenda

    canvas.draw()

def average_height( y):
    # Calculamos la magnitud de la desviación absoluta

    abs_deviation = np.abs(y)
    # Calculamos Ra
    #L = np.max(x) - np.min(x)
    ave = np.mean(abs_deviation)
    return ave

def average_per_lenght(y):
    if len(y)==1:
        return y[0]
    return np.mean(y)
def quadratic_average(x, y):
    L = np.max(x) - np.min(x)
    # Calculaos el valor RMS ----------
```

```
    cuadratic_deviation = np.square(y)
    qms = np.sqrt(abs((1 / L) * integrate.simps(cuadratic_deviation, x)))
    return qms

def PeakAndValleyHigher( y):
    minimum=np.min(y)
    maximum=np.max(y)
    return minimum, maximum


def DistanceInPeakAndValley(min, max):
    return abs(min)+abs(max)



root = tk.Tk()
root.title('Form, Profile, Waviness and Roughness')



frame1 = tk.Frame(root)
frame1.pack(side=tk.TOP)

lambda_label = tk.Label(frame1, text='Sigma:')
lambda_label.pack(side=tk.LEFT)

lambda_entry = tk.Entry(frame1)
lambda_entry.insert(0, str(lambdaCutoff))
lambda_entry.pack(side=tk.LEFT)
```

```
alpha_label = tk.Label(frame1, text='LambdaCutoff(mm):')
alpha_label.pack(side=tk.LEFT)

alpha_entry = tk.Entry(frame1)
alpha_entry.insert(0, str(lambdaCutoff))
alpha_entry.pack(side=tk.LEFT)


button = tk.Button(frame1, text='Plot', command=update_plot)
button.pack(side=tk.LEFT)

frame2 = tk.Frame(root)
frame2.pack(side=tk.TOP, fill=tk.BOTH, expand=True)


fig, axs = plt.subplots(4, 1, sharex=True, figsize=(5, 8))


canvas = FigureCanvasTkAgg(fig, master=frame2)
canvas.draw()
canvas.get_tk_widget().pack(side=tk.TOP, fill=tk.BOTH, expand=1)

# Crear la barra de herramientas
toolbar = NavigationToolbar2Tk(canvas, frame2)
toolbar.update()

fig.text(0.5, 0.04, 'µm', ha='center', va='center')
```

```
fig.text(0.06, 0.5, 'µm', ha='center', va='center', rotation='vertical')

f_gaussian = gaussian_filter1d(y, sigma=20, mode='nearest')
f_roughness = GetRoughness(f_gaussian, y)

f_profile = interp1d(x, y, kind='quadratic')

func_gaussian = interp1d(x, f_gaussian, kind='quadratic')
func_roughness = interp1d(x, f_roughness, kind='quadratic')



#area=integrate(f_profile(x))

for ax in axs:
    ax.set_ylim(min(y), max(y))



data = {"Form": (PixelInX ,PixelInY, "black"),
        "Profile": (x, f_profile(x), "blue"),
        "Waviness": (x, func_gaussian(x), "orange"),
        "Roughness": (x, func_roughness(x), "red")}




# Iterar sobre los subplots y los datos correspondientes
for ax, (title, (x, ydata, color)) in zip(axs, data.items()):
    if title=="Form":
        ax.scatter(PixelInX*unit, PixelInY*unit, label='Form', s=SizeOfPoint(PixelInX))
```

```
        ax.set_yticklabels([])
        axs[0].axhline(y=0, color="black")
        # axs[0].scattr(x, poly(x), label="Form")
        ax.set_title("Form")
        ax.set_ylim(min(PixelInY*unit), max(PixelInY*unit))
        ax.legend(markerscale=30)

    else:
        ax.plot(x, ydata, label=title, color=color, linestyle="dashdot")  # Plotear los datos
        ax.axhline(y=0, color="black")  # Agregar una línea horizontal en y=0
        #ax.axvline(x=500, color="black")
        ax.set_title(title)  # Establecer el título del subplot
        ax.axhline(y=average_height(ydata), color="red", linestyle="--",
            label=title[0]+"a = {:.3f}".format(average_height(ydata)))  # Agregar la línea de la media
aritmética
        ax.axhline(y=quadratic_average(x, ydata), color="green", linestyle="--",
            label=title[0]+"q = {:.3f}".format(quadratic_average(x, ydata)))  # Agregar la línea de la
media cuadrática

        minValley=PeakAndValleyHigher(ydata)[0]
        maxValley=PeakAndValleyHigher(ydata)[1]

        ax.axhline(y=minValley, color="red", linestyle="-",
                label=title[0] + "max valley = {:.3f}".format(PeakAndValleyHigher(ydata)[0]),
linewidth=2)

        ax.axhline(y=maxValley, color="green", linestyle="-",
                label=title[0] + "max peak = {:.3f}".format(PeakAndValleyHigher(ydata)[1]),
linewidth=2)
```

```
    ax.axhline(y=DistanceInPeakAndValley(minValley, maxValley), color="purple", linestyle="-",
               label=title[0] + "z = {:.3f}".format(DistanceInPeakAndValley(minValley, maxValley)), linewidth=0)


    ax.legend()
    #ax.legend(labels=title[0] + "z = " + str(DistanceInPeakAndValley(minValley, maxValley)))
    #ax.legend(label=title[0]+"z = "+ DistanceInPeakAndValley(minValley, maxValley))  # Agregar la leyenda



# Iniciar la aplicación
root.mainloop()
```

VITA

Jesus Rivas graduated with a bachelor's in mechanical engineering from the Universidad Autonoma de Ciudad Juarez and a master's in manufacturing from the University of Texas at El Paso. Jesus has more than 7 years of design, engineering, and development expertise from companies that are leaders in the automotive industry, such as Delphi and Valeo. He received certifications in ASME Geometrical and Dimension Tolerancing (GD&T), Systems Engineering, Six Sigma Green Belt, and Robust Engineering.

Contact Information Rivas_132@Hotmail.com